IEEE Access
Multidisciplinary | Rapid Review | Open Access Journal

Received 7 January 2024, accepted 15 January 2024, date of publication 23 January 2024, date of current version 6 February 2024.

*Digital Object Identifier 10.1109/ACCESS.2024.3357628*

RESEARCH ARTICLE

# Radio Modulation Classification Optimization Using Combinatorial Deep Learning Technique

**ZIAD ELKHATIB[1], (Member, IEEE), FIRUZ KAMALOV[1], (Member, IEEE), SHERIF MOUSSA[1], (Member, IEEE), ADEL BEN MNAOUER[2], (Member, IEEE), MUSTAPHA C.E. YAGOUB[3], (Senior Member, IEEE), AND HALIM YANIKOMEROGLU[4], (Fellow, IEEE)**

[1]Department of Electrical and Computer Engineering, Canadian University Dubai, Dubai, United Arab Emirates
[2]Department of Computer Science Engineering, Prince Sultan University, Riyadh 66833, Saudi Arabia
[3]Department of Electrical and Computer Engineering, University of Ottawa, Ottawa, ON K1N 6N5, Canada
[4]Department of Electrical and Computer Engineering, Carleton University, Ottawa, ON K1S 5B6, Canada

Corresponding author: Ziad Elkhatib (ziad.elkhatib@cud.ac.ae)

**ABSTRACT** We present an automatic signal modulation classification model using combinatorial deep learning technique. Our proposed deep learning model increase accuracy for low Signal-to-Noise Ratio (SNR) and maintain a high classification accuracy for high SNR signals. Using a hybrid deep learning model combining both ConvLSTM with Transformer-block neural networks, the proposed modulation classifier architecture can learn the signal for both low and high SNR and get better accuracy for signals with high noise. The proposed deep learning modulation classification technique achieves improved classification accuracy of 66% for low SNR signals and 93.5% at high SNR showing that our model is robust under noisy signal modulation. Thus, getting better accuracy in lower SNR signals without sacrifice accuracy for higher SNR signals. An adaptive weighted focal loss function is proposed as an optimized loss function for efficient classification which can be used to control the outliers within a class imbalance and avoid underflow issues. Our deep learning radio modulation classification model works using raw signal without the need of denoising the noisy signal.

**INDEX TERMS** Automatic modulation classification, dynamic spectrum allocation, deep learning techniques, transformer-block ConvLSTM, feature-based extraction, AI-based wireless communications.

## I. INTRODUCTION

Automatic signal modulation recognition in AI-based wireless communication can be done using combinatorial deep learning techniques to improve resource shortage and spectrum utilization efficiency for dynamic spectrum allocation [1]. A clean signal will have a high Signal-to-Noise Ratio (SNR). We should be able to classify signals in both low and high SNR. Our proposed deep learning model increase accuracy for low SNR and maintain a high classification accuracy for high SNR signals. Using a hybrid deep learning model by combining both ConvLSTM with Transformer-block neural networks shown in Fig. 1. The proposed deep learning modulation classification technique achieves improved classification accuracy of 66% for low SNR signals and 93.5% at high SNR. Thus, getting better accuracy in lower SNR signals without sacrifice accuracy for higher SNR signals. Simulation results show that our proposed deep learning model is robust under noisy signal modulation without the need of denoising the noisy signal.

By utilizing combinatorial technique in our proposed model that incorporates both ConvLSTM and transformer-block model. Our proposed model has advantage in using transformer-block network since it uses parallelization processing thus make use of parallel computation [2]. Also, the input size can be any size or vector length and simultaneously

The associate editor coordinating the review of this manuscript and approving it for publication was Barbara Masini.

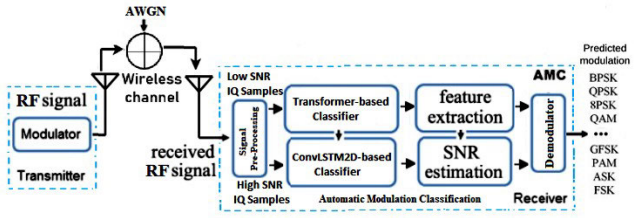


**FIGURE 1. Automatic modulation classification model using combinatorial deep learning technique for both low and high SNR signal classification.**

proceed by the transformer-block network instead of sequentially hence solving the vanishing gradient problem. By using transformer-block network in our proposed model, the context of data can be well captured because it uses the positional encoding and self-attention mechanism which are included in the network modules [2].

## II. NEURAL-NETWORK MODULATION CLASSIFICATION

Automatic modulation classification (AMC) offers spectrum management and interference detection for software defined radio and cognitive radio networks [1].

As a practical solution to improve the effectiveness of automatic modulation classification, deep learning techniques have been widely used in wireless communication systems. Automatic modulation classification can be divided into likelihood-based and feature-based methods [1]. The likelihood-based method requires more computational complexity. Whereas feature-based method requires less computational complexity [3], [4], [5], [6].

The signal is not ideal and is usually combined with noise. A noisy signal will have a low SNR [3], [4], [5], [6]. It means that if the noise is higher, the model will likely to fail to do the modulation classification. We should be able to classify signals both in low SNR and high SNR.

The authors West and O'Shea [7] combined CNN and RNN neural networks to form a CLDNN model which improved the modulation recognition accuracy to 85% in high SNR only. The authors Chen et al. [8] combined CNN, RNN, and GAN neural networks to extract the signal spatial characteristics and classification is done with a fully connected layer achieving an accuracy of more than 90% in high SNR only. Jiang et al. [9] combined CLDNN with LSTM neural network achieving 90.8% accuracy at high SNR. Tang et al. [10] combined CNN with GAN achieving an accuracy of 100% at high SNR. Xu et al. [11] combined CNN with LSTM neural networks achieving an accuracy of 90% at high SNR. Jiang et al. [12] combined CNN with Bi-LSTM achieving an accuracy of 93.1%. Liang et al. [13] combined ResNeXt with Attention block achieving an accuracy of 90% in high SNR. Chang et al. [14] combined CNN with Bi-GRU achieving an accuracy of 84% in high SNR only.

Zhang et al. [15] combined GRU with CNN achieving an accuracy of 99.4%.. Zou et al. [16] combined CLDNN with Attention achieving an accuracy of 90% in high SNR. The authors Bai et al. [17] combined ResNet with CNN achieving an accuracy of 91% in high SNR. Chen et al. [8] used a deep learning-based attention framework using CNN, RNN, and GAN neural networks. The CNN and RNN are used to extract the signal spatial characteristics. Zou et al. [16] used Attention along with CLDNN neural networks model achieving an accuracy of 90% in high SNR. Bai et al. [17] combined complex value network with ResNet model achieving an accuracy of 91% at high SNR. Chang et al. [14] combined CNN with Bi GRU networks achieving an accuracy of 84% at high SNR. Duan et al. [18] used combination of CNN with BiLSTM and Attention models achieving an accuracy of 93% at high SNR. Xu et al. [11] combined CNN and LSTM with FC models achieving an accuracy of 90% at high SNR.

Dampage et al. [19] used both LSTM and Bi LSTM models achieving an accuracy of 90% at high SNR. Liu et al. [20] combined DCN and BiLSTM models achieving an accuracy of 90% at high SNR. Yang et al. [21] used an IRS model combined with LSTM neural networks achieving an accuracy of 90% at high SNR. Kumaran et al. [22] combined GRU and BiLSTM neural networks achieving an accuracy of 92% at high SNR. Ze and Vikalo [23] used single neural network model LSTM achieving an accuracy of 90% at high SNR. Xie et al used DNN neural network model to extract sixth order cumulant feature of the signal achieving an accuracy of 92% at high SNR. Zhang et al. [24] used BP network model achieving an accuracy of 98% at high SNR. Our proposed deep learning model increase accuracy for low SNR and maintain a high classification accuracy for high SNR signals compared to previous published work. Using a hybrid deep learning model by combining both ConvLSTM with Transformer-block neural networks. Our proposed deep learning modulation classification technique achieves improved classification accuracy of 66% for low SNR signals and 93.5% at high SNR. Other published work such as Oikonomou [25] do not use deep learning models and hence do not have the capability of modulation recognition format prediction also they do not have the capability of loading automatic modulation recognition deep learning model on hardware accelerator chips to take processing load of the main hardware processor compared to our proposed deep learning model [25]. Our proposed automatic modulation recognition format prediction combined deep learning model can be loaded on a hardware accelerator chip thus take the processing load of the main hardware microprocessor.

Recent studies show that deep learning models such as neural networks can extract features effectively from various representation of wireless signals such as in-phase and quadrature (IQ) signal or spectrogram in order to achieve high modulation classification accuracy [3], [4], [5], [6].

The received signals is preprocessed from I/Q signals cartesian coordinates to polar coordinates to the corresponding amplitude and phase in order to extract more features. By learning more features from the polar domain makes the network more resilient to fading channels [3], [4], [5], [6] then are converted to Fig. 2 which describes the constellation

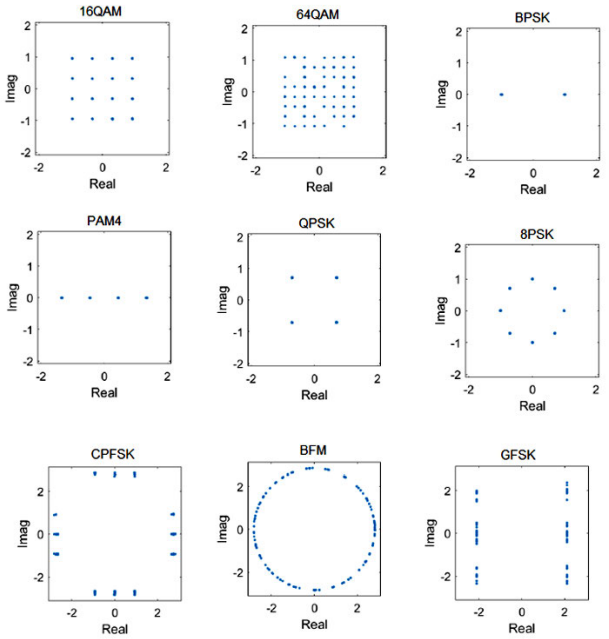


**FIGURE 2.** Various modulation constellation data signals are represented by two vectors one for quadrature and other for In-phase.

diagrams of common modulation modes after coordinate transformation.

Fig. 2 shows various modulation constellation data signals considered in this work that are represented by two vectors one for Quadrature and In-phase representation. Similar modulation constellation data signals are considered in previous publish work Bell [3] where they combined both ResNet and CNN achieving 86% accuracy in high SNR only unlike our proposed work where we achieve high accuracy in both high and low SNR. Also Huang [4] used similar modulation constellation data signals in their published work using compressive CNN achieving accuracy of 95% accuracy in high SNR only. Guo [5] also used similar modulation constellation data signals in their published work using Residual CNN achieving accuracy of 92% accuracy in high SNR only unlike our proposed work where we achieve high accuracy in both high and low SNR.

Zhang et al. [6] proposed a multiscale CNN for constellation-based modulation classification. The network structure was composed of multiple processing modules achieving a classification accuracy can reach 97.7% in high SNR only [6] [26]. Shi et al. [27] [26] proposed an automatic modulation recognition (AMR) method which includes a multi-scale convolution deep network for recognizing modulation types achieving an overall recognition accuracy of 98.7%.again only in high SNR unlike our proposed work where we achieve high accuracy in both high and low SNR [27] [26].

## III. FEATURE EXTRACTION-BASED CLASSIFICATION

The proposed deep-learning-based model for automatic modulation classification (AMC) was trained using IQ component signals and image-based constellation diagrams [3], [4], [5], [6].

The feature-based method usually requires less computational complexity by extracting data representation features for classification [3], [4], [5], [6]. Key features can be categorized as time-domain features including instantaneous amplitude, phase and frequency and frequency-domain features such as wavelet transform of the signals, higher order moments (HOMs) and higher order cumulants (HOCs) that are described in (1) through (50) as follows [3], [4], [5], [6].

The BPSK transmitter emits a signal with voltage of "$-a$" volts when transmitting bits X=0 and the random variable X is mapped to voltage of "$+a$" volts when transmitting bits X=1. The communication channel adds the Gaussian noise to this transmitted signal. Therefore, the conditional distribution and variance of $\sigma_{\mathrm{n}}^2$ with Gaussian distribution $p\,(r)$ is the Gaussian distribution with mean "$-a$" volts variance of $\sigma_{\mathrm{n}}^2$ given by and is represented as follows [28]

$$p\,(r) = \frac{1}{\sqrt{2\pi\sigma_n^2}} \exp\left(-\frac{1}{2}\left(\frac{r+a}{\sigma_n}\right)^2\right). \tag{1}$$

The ratio when transmitter sends X=0 to X=1 is given by the following $\lambda$ and is represented as follows [28]

$$\lambda = \frac{\frac{1}{\sqrt{2\pi\sigma_n^2}} \exp\left(-\frac{1}{2}\left(\frac{r-a}{\sigma_n}\right)^2\right)}{\frac{1}{\sqrt{2\pi\sigma_n^2}} \exp\left(-\frac{1}{2}\left(\frac{r+a}{\sigma_n}\right)^2\right)}. \tag{2}$$

which simplifies to the following equation if $\lambda > 1$ the receiver estimates that X=1 is sent else X=0 [28]

$$\lambda = \exp\left(\frac{2ra}{\sigma_n^2}\right). \tag{3}$$

which is evaluated to

$$\log\left(\lambda\right) = \frac{2ra}{\sigma_n^2}. \tag{4}$$

The heterodyne Zero-IF receiver shown in Fig. 3 have a decision rule that can be written in a minimum distance which compares the squared Euclidean distances $\mathrm{d}_1^2$ and $\mathrm{d}_0^2$ and is represented as follows [28]

$$d_1^2 - d_0^2 = (r-a)^2 - (r+a)^2 \tag{5}$$

Various features extracted from IQ signal components, such as amplitude and phase, higher order statistics and higher order cumulants are utilized to provide sequence classification [3], [4], [5], [6].

A feature extraction-based classification method usually includes two stages data feature extraction and classifier decision making. The key features can be categorized as time domain features including amplitude, frequency, and transform domain features such as higher-order moments (HOMs) and higher-order cumulants (HOCs).

Coefficients series expansion are expected values of complex-valued polynomials H(z). They are computed using the input symbols cross-moments. These input symbols

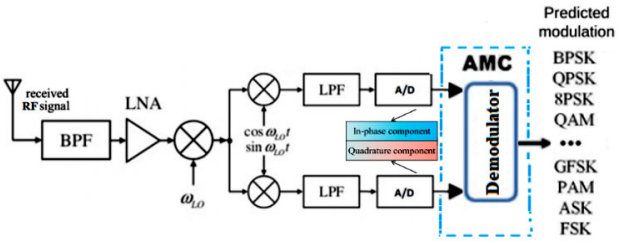


**FIGURE 3.** Deep learning-based radio modulation recognition for heterodyne Zero-IF receiver with quadrature down conversion.

cross-moments used to determine the probability density function the symbols came from. The Gram-Charlier expansion series can be defined as follows [29]

$$f_z(z) = \sum_{p=0}^{\infty} \sum_{q=0}^{\infty} \frac{E\left[H_{p,q}(z)\right]^*}{\sqrt{p!q!}} \frac{H_{p,q}(z)}{\sqrt{p!q!}} \frac{1}{\pi} e^{-zz^*} \quad (6)$$

Some complex Hermite polynomials are given by the following coefficients [29]

$$H_{0,0}(z) = 1 \quad (7)$$
$$H_{1,0}(z) = z \quad (8)$$
$$H_{1,1}(z) = |z|^2 - 1. \quad (9)$$
$$H_{2,1}(z) = z^2 z^* - 2z. \quad (10)$$
$$H_{2,2}(z) = |z|^4 - 4|z|^2 + 2. \quad (11)$$

The density functions can be determined by the infinite sequence of these coefficients and can be defined as follows [29].

$$h_{p,q}(f_z) = \frac{E\left[H_{p,q}(z)\right]^*}{\sqrt{p!q!}}. \quad (12)$$

The Euclidean distance between two density function or sequence coefficient is determined as follows [29]

$$d(f_1, f_2) = \sqrt{\sum_{p=0}^{\infty} \sum_{q=0}^{\infty} |h_{p,q}(f_1) - h_{p,q}(f_2)|^2}. \quad (13)$$

This Euclidean metric on the set of Gram-Charlier coefficients enables use of metric space-based classifiers.

We can define the second-order moments of a stationary random process y(n) with the following coefficients. $C_{40}$, $C_{41}$, or $C_{42}$ can be determined in terms of the fourth-and second order moments of y(n) as follows [30], [31]

$$C_{21} = \frac{1}{N} \sum_{n=1}^{N} |y(n)|^2. \quad (14)$$
$$C_{20} = \frac{1}{N} \sum_{n=1}^{N} y^2(n). \quad (15)$$

The higher order cumulants (HOCs) of fourth order are used for automatic modulation classification. The cumulants of the received symbol y are determined as follows [30], [31]

$$C_{40} = \frac{1}{N} \sum_{n=1}^{N} y^4(n) - 3C_{20}^2. \quad (16)$$
$$C_{41} = \frac{1}{N} \sum_{n=1}^{N} y^3(n) y^*(n) - 3C_{20}C_{21}. \quad (17)$$
$$C_{42} = \frac{1}{N} \sum_{n=1}^{N} |y(n)|^4 - C_{20}^2 - 2C_{21}^2. \quad (18)$$

We can estimate the normalized cumulants as such. By using the above (14) to (18), three HOC feature parameters (i.e., F1, F2, and F3) are extracted for classification and represented as follows [30], [31]

$$F_1 = \frac{|C_{40}|}{C_{42}} \quad (19)$$
$$F_2 = \frac{|C_{41}|}{C_{42}} \quad (20)$$
$$F_3 = \frac{|C_{63}|^2}{|C_{42}|^3} \quad (21)$$

$C_{40}$ is utilized to decide whether the constellation diagram is for the real valued rectangular QAM or circular PSK or BPSK or PAM. The amount of cumulative is used to determine the type of modulation. We choose the decision limits as illustrated as follows [30], [31]

$$C_{40} < 0.34 \text{ implies PSK.} \quad (22)$$
$$0.34 < C_{40} < 1.02 \text{ implies QAM.} \quad (23)$$
$$1.02 < C_{40} < 1.68 \text{ implies PAM.} \quad (24)$$
$$1.68 < C_{40} < 1.68 \text{ implies BPSK.} \quad (25)$$

Thus, the lowest value of distance between empirical cumulants and theoretical values ($L \to \infty$) indicates the utilized modulation type.

The signal received by the receiver can be described as follows.

Under the assumption that the signal received by the receiver has undergone carrier synchronization, symbol timing, and matched filtering, and the channel noise is Gaussian white noise, the symbol synchronous sampling complex signal sequence obtained at the output is [32]

$$\begin{aligned} x(t) &= s(t) + n(t) \\ &= \sqrt{A} \sum_{k}^{g} \mu_k \sqrt{E_n} \lambda(\mathrm{t} - \mathrm{nT}) \exp[j(2\pi f_c + O_c] + n(t) \end{aligned} \quad (26)$$

x (t) is the signal received at the receiving end, and s (t) is the signal at the transmitting end, n (t) is the zero-mean complex Gaussian white noise, $E_n$ is signal energy.

where k=1,2 ...g, and g is the length of the transmitted code element sequence. A is the unknown factor amplitude, $\lambda$ (t) is transmitted waveform code element; $\mu_k$ is code sequence element, $O_c$ is carrier phase, Ts is width of the code element, $E_n$ is signal energy and $f_c$ is carrier frequency [32].

For zero-mean stationary random process X (t) , the p-order mixing moment and k-order HOC are defined as follows.

The characteristic parameters HOCs for various signals that can be designed in accordance is shown in Table 1. Utilizing the following equations three feature parameters

**TABLE 1.** High-order cumulant HOC modulation signals.

| Signal | $\|C_{40}\|$ | $\|C_{41}\|$ | $\|C_{42}\|$ | $\|C_{63}\|$ |
|---|---|---|---|---|
| 2ASK | $2E_n^2$ | $2E_n^2$ | $2E_n^2$ | $16E_n^3$ |
| 4ASK | $1.36E_n^2$ | $1.36E_n^2$ | $1.36E_n^2$ | $8.32E_n^3$ |
| 4PSK | $E_n^2$ | 0 | $E_n^2$ | $4E_n^2$ |
| *2FSK* | 0 | 0 | 0 | $4E_n^3$ |
| *16QAM* | $0.68E_n^2$ | $0.68E_n^2$ | $0.68E_n^2$ | $2.08E_n^3$ |
| *64QAM* | $0.62E_n^2$ | $0.62E_n^2$ | $0.62E_n^2$ | $1.08E_n^3$ |

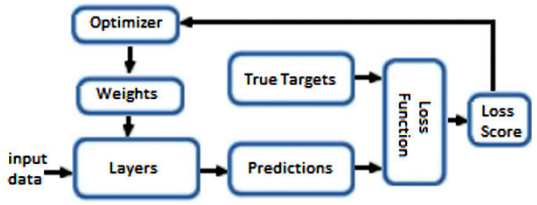


**FIGURE 4.** Classification loss function optimization.

(i.e., F1, F2, and F3) are extracted [31]

$$F_1 = \frac{|C_{40}|}{C_{42}} \tag{27}$$

$$F_2 = \frac{|C_{41}|}{C_{42}} \tag{28}$$

$$F_3 = \frac{|C_{63}|^2}{|C_{42}|^3} \tag{29}$$

The three signal features extracted from HOC having strong low SNR robustness where $E_n$ is signal energy [32].

The SNR estimated value can be defined as follows [32]

$$SNR = \frac{\sqrt{2M_2^2 - M_4}}{M_2 - \sqrt{2M_2^2 - M_4}}. \tag{30}$$

The second-order moment M2 and fourth order moment M4 method are given by [32]

$$M_2 = \frac{1}{N}\sum_{n=0}^{N-1} |x(n)|^2. \tag{31}$$

$$M_4 = \frac{1}{N}\sum_{n=0}^{N-1} |x(n)|^4. \tag{32}$$

N is the signal length, and the received signal is x(n).

Then we perform normalization to the data by minimizing the penalty function is how Neural networks learn. And accordingly, they iteratively updates a series of weights and biases. Weights in loss function can be used to control the outliers for positive predictions to deal with a class imbalance as shown in Fig. 4.

The weighted cross-entropy loss function can be determined with the following equation. Where $y_i$ is actual value of y and $y_i'$ is predicted value of y, w is the weight associated with each sample, M is the total number of samples in the dataset,

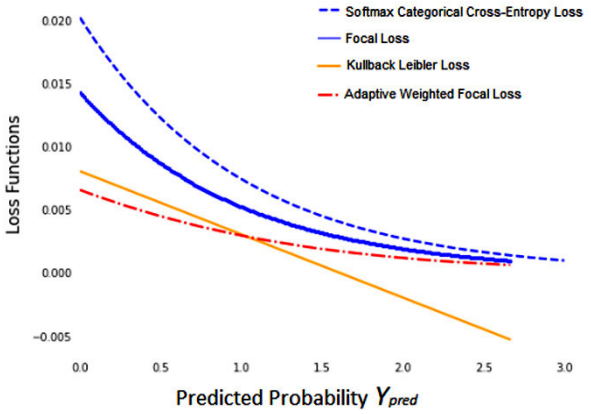


**FIGURE 5.** Loss function optimization analysis.

N is the normalization factor for sample [2], [33], [34]

$$L\left(y_i', y_i\right) = -\frac{\sum_{i=1}^{M} \omega_i \sum_{i=1}^{M} \frac{y_i}{N_i} \log y_i'}{\sum_{i=1}^{M} \omega_i}. \tag{33}$$

A categorical cross-entropy loss function use softmax instead of using sigmoid as the last layer activation. The categorical cross-entropy loss function can be determined as follows where M is the total number of samples in the dataset [31], [33] [34]

$$L\left(y_i', y_i\right) = -\sum_{i=1}^{M} y_i \log y_i'. \tag{34}$$

In focal loss function has the same softmax of cross-entropy except it is an index of which category is true instead of the target being a probability distribution. The index of which category is the true value we just pass in as follows where M is the total number of samples in the dataset and $\Upsilon$ is the hyperparameter [31], [33] [34].

$$L\left(y_i', y_i\right) = -\sum_{i=1}^{M} (1 - y_i')^{\Upsilon} y_i \log y_i'. \tag{35}$$

To avoid underflow issues the Kullback Leibler loss function expects the argument input in the log-space and is computed as follows where M is the total number of samples in the dataset [31], [33] [34]

$$L\left(y_i', y_i\right) = \sum_{i=1}^{M} y_i(\log y_i - \log y_i'). \tag{36}$$

An adaptive weighted focal loss is proposed as an optimized loss function for efficient classification which can be used to control the outliers with class imbalance and avoid underflow issues as shown in Fig. 5 and it can be determined as follows where $Y_{pred}$ is the predicted probability representing the model's estimated probability that a sample belongs to the positive class [31], [33] [34]

$$L\left(y_i', y_i\right) = -\frac{\sum_{i=1}^{M} \omega_i \sum_{i=1}^{M} \frac{(1-y_i')^{\lambda}}{N_i} (\log y_i - \log y_i')}{\sum_{i=1}^{M} \omega_i}. \tag{37}$$

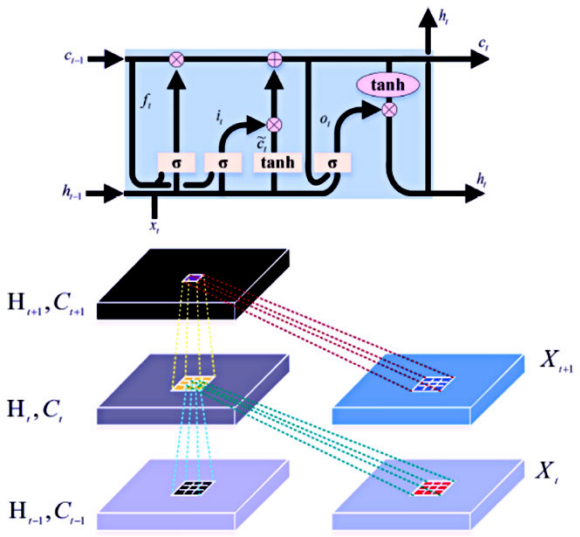


**FIGURE 6.** ConvLSTM memory cell structure.

## IV. PROPOSED MODULATION CLASSIFICATION DEEP LEARNING MODEL

In this section, a hybrid combinatorial deep learning model combining both ConvLSTM with Transformer-block neural networks is proposed. Our proposed modulation classifier architecture can learn the signal for both low and high SNR and get better accuracy for signals with high noise. For learning persistent features from a time series data, Recurrent Neural Networks (RNN) are utilized. However, these models using RNNs suffer from much slower training time. LSTM efficient in learning long-term dependencies is a special type of RNN. ConvLSTM Convolutional Long Short-term is a special type of RNN which integrates both CNN with LSTM. ConvLSTM is a modification and extended version of LSTM as shown in Fig. 6.

The data transmission and processing in LSTM are realized by three key gate units: input gate, output gate, and forget gate, which are used for implementing information processing.

In LSTM, the input gate $i_t$, the output gate $o_t$, and forgotten gates $f_t$ are defined as [19], [20], [35], and [36], respectively

The equations of LSTM cell are as follows. The input gate and memory status update information are [19], [20], [23] [35],

$$i_t = \sigma(\mathrm{W_{xi}X_t + W_{hi}H_{t-1} + W_{ci}C_{t-1} + b_i}). \quad (38)$$

$$f_t = \sigma(\mathrm{W_{xf}X_t + W_{hf}H_{t-1} + W_{cf}C_{t-1} + b_f}). \quad (39)$$

$$o_t = \sigma(\mathrm{W_{xo}X_t + W_{ho}H_{t-1} + W_{co}C_t + b_o}). \quad (40)$$

where $\sigma$ is a sigmoid function and $\mathrm{X_t}$ is the input to the current gate structure, and $\mathrm{H_{t-1}}$ is the output of the previous gate memory cell structure. $\mathrm{C_{t-1}}$ represent the state of the last memory cell in LSTM. $\mathrm{W_{xi}}$ and $\mathrm{b_i}$ are the weight and bias of the input gate, $\mathrm{W_{xf}}$ and $\mathrm{b_f}$ are the weight and bias of the forget gate, and $\mathrm{W_{xo}}$ and $\mathrm{b_o}$ are the weight and bias of the output gate [19], [20], [23].

The input feature sequence $\mathrm{X_t}$ and the output sequence of the previous time $\mathrm{H_{t-1}}$ are input to the memory cell. The forgetting factor $f_t$ is obtained via the forgetting gate. tanh is an activation function that generates candidate values $\tilde{C}_t$. In addition, $\tilde{C}_t$ participates in the calculation to obtain the memory state $\mathrm{C_t}$ [19], [20], [23]

$$\tilde{C}_t = tanh(\mathrm{W_{xc}X_t + W_{hc}H_{t-1} + b_c}). \quad (41)$$

$$c_t = f_t.C_{t-1} + i_t.\tilde{C}_t. \quad (42)$$

$$h_t = \sigma_t.\tanh(c_t). \quad (43)$$

The output gate control factor $o_t$ determines whether to output information and is expressed as follows [35]

$$o_t = \sigma(\mathrm{W_{xo}X_t + W_{ho}H_{t-1} + W_{co}C_t + b_o}). \quad (44)$$

Compared with $\mathrm{C_t}$, $\mathrm{H_{t-1}}$ contains more information about the current moment. Therefore, $\mathrm{H_{t-1}}$ represents short-term memory, while $\mathrm{C_t}$ represents long-term memory and the state-update is given by the following equations [19], [20], [23]

The Convolutional Long Short-term ConvLSTM shown in Fig. 6 calculation equations can be expressed as [37]

$$i_t = \sigma(\mathrm{W_{xi*}X_t + W_{hi*}H_{t-1} + W_{ci}oC_{t-1} + b_i}). \quad (45)$$

$$f_t = \sigma(\mathrm{W_{xf*}X_t + W_{hf*}H_{t-1} + W_{cf}oC_{t-1} + b_f}). \quad (46)$$

$$o_t = \sigma(\mathrm{W_{xo*}X_t + W_{ho*}H_{t-1} + W_{co}oC_t + b_o}). \quad (47)$$

$$\tilde{C}_t = tanh(\mathrm{W_{xc*}X_t + W_{hc*}H_{t-1} + b_c}). \quad (48)$$

$$c_t = f_t o\mathrm{C_{t-1}} + i_t o\tilde{C}_t. \quad (49)$$

$$H_t = \sigma_t o\tanh(C_t). \quad (50)$$

where $\mathrm{X_t}$ denotes the input of the current cell, $\mathrm{C_{t-1}}$ and $\mathrm{H_{t-1}}$ are state and output of the last cell, respectively. The $*$ operator means the convolution operation and the o denotes the Hadamard product. W denotes the convolution filter. $\mathrm{W_{xi}}$ and $\mathrm{b_i}$ are the weight and bias of the input gate, $\mathrm{W_{xf}}$ and $\mathrm{b_f}$ are the weight and bias of the forget gate, and $\mathrm{W_{xo}}$ and $\mathrm{b_o}$ are the weight and bias of the output gate [37]. ConvLSTM Convolutional Long Short-term contains convolution operation inside it and is used extract spatial-spectral features [37]. It captures long-term and short-term dependencies by stacking multiple ConvLSTM layers [37]. We should be able to classify signals both in low SNR and high SNR. We proposed a combined deep learning architecture shown in the Fig. 7 that works to handle the noisy signal modulation low SNR signal modulation and maintain high accuracy for High SNR signals. Adding more ConvLSTM layers with MaxPooling layers can extract more features which is fed into classification layer to predict the probability distribution of each modulation class and is given by the following [37], [38], [39].

$$P(y = i|x, W, b) = \frac{e^{(\omega_{jx}+b_j)}}{\sum_{j=1}^{N} e^{(\omega_{jx}+b_j)}}. \quad (51)$$

W is weight and b is the bias of the classification layer with a loss function determined as [37], [40]

$$L(y_i, y_i') = -\sum_{i=1}^{M} (y_i.\log y_i'). \quad (52)$$

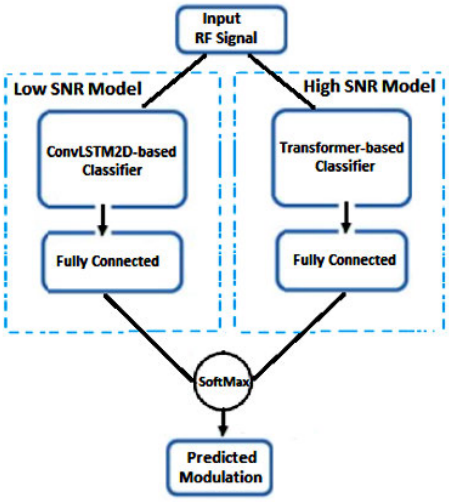


**FIGURE 7.** Combinatorial deep learning neural networks model for both low SNR and high SNR modulation classification.

**TABLE 2.** ConvLSTM network model layers.

| Layer type | Output Shape |
|---|---|
| Input | 128x2 |
| *Conv1D* | 121x64 |
| *MaxPooling1D* | 60x64 |
| *ConvLSTM* | 60x64 |
| *Dropout* | 60x64 |
| *ConvLSTM* | 60x64 |
| *Dropout* | 64 |
| *GlobalAveragePooling1D* | 64 |
| *Dense* | 20 |
| *Dropout* | 20 |
| *Dense (Softmax)* | 11 |

Our proposed architecture uses two streams as shown in Fig. 7, first stream with ConvLSTM and second stream with transform-block network to extract features for high and low SNR signals. Our proposed model has advantage in using transformer-block network since it uses parallelization processing thus make use of parallel computation [2]. Also, the input size can be any size or vector length and simultaneously proceed by the transformer-block network instead of sequentially hence solving the vanishing gradient problem. By using transformer-block network in our proposed model, the context of data can be well captured because it uses the positional encoding and self-attention mechanism which are included in the network modules [2].

The layer type and output shape for ConvLSTM network structure specific to each layer that is implemented is shown in Table 2. As illustrated in Table 2 a Conv1D convolutional layer consisting of 64 filters is applied to the $128 \times 2$ IQ inputs with kernel size of 8.

For higher resolution we need a large filter. It maps the input IQ components onto feature channels. Then, based on the characteristics of IQ signal. Softmax is used as the activation function for multi-class classification and the optimizer used is Adam with loss function categorical cross entropy along with learning rate of 0.01.

**TABLE 3.** ConvLSTM2D network model layers.

| Layer type | Output Shape |
|---|---|
| Input | 128x2 |
| *Conv2D* | 121x64 |
| *MaxPooling2D* | 60x64 |
| *ConvLSTM2D* | 60x64 |
| *Dropout* | 60x64 |
| *ConvLSTM2D* | 60x64 |
| *Dropout* | 64 |
| *GlobalAveragePooling2D* | 64 |
| *Dense* | 20 |
| *Dropout* | 20 |
| *Dense (Softmax)* | 11 |

After that a MaxPooling1D and then a ConvLSTM and dropout layer follows with the same parameters. After that second ConvLSTM and a dropout layer followed by a *GlobalAveragePooling1D* with the same parameters and a Dense and Dropout layer. At the end is a fully connected layer with an output size 11 with a Softmax activation function.

To increase the overall accuracy performance of our proposed model a ConvLSTM2D model is implemented. The layer type and output shape for ConvLSTM2D network structure specific to each layer that is implemented is shown in Table 3. The proposed architecture consists of an input layer of $128 \times 2$ IQ input, followed by a Conv2D layer with 64 filters and 8 kernels then a MaxPooling2D layer and then a ConvLSTM2D and a Dropout layer follows with the same parameters. After that second ConvLSTM2D and a Dropout layer followed by a *GlobalAveragePooling2D* with the same parameters and a Dense and Dropout layer. At the end is a fully connected layer with an output size 11. Softmax is used as the activation function for multi-class classification and the optimizer used is Adam with loss function categorical cross entropy along with learning rate of 0.01.

A Transformer-block is utilized as the second stream for larger training data set parallelization [41] [42]. Transformers use attention blocks resulting in faster training time and inference testing time. Our proposed model has advantage in using transformer-block network since it uses parallelization processing thus make use of parallel computation [2]. The final network design for our proposed classifier model combine Transformer-block with ConvLSTM2D as shown in Fig. 8 and Fig. 9 to achieve higher classification accuracy for both Low and High SNR signals. The proposed multi-stream network can extract various characteristics of signals as shown in Fig. 9.

To determine the transformer self-attention, we use the following [2], [43]

$$\text{Attention}(Q, K, V) = \text{softmax}\left(\frac{QK^T}{\sqrt{d_k}}\right)V. \quad (53)$$

where Q is the query sequence and K is the keys in the sequence and V is the sequence value. And the attention

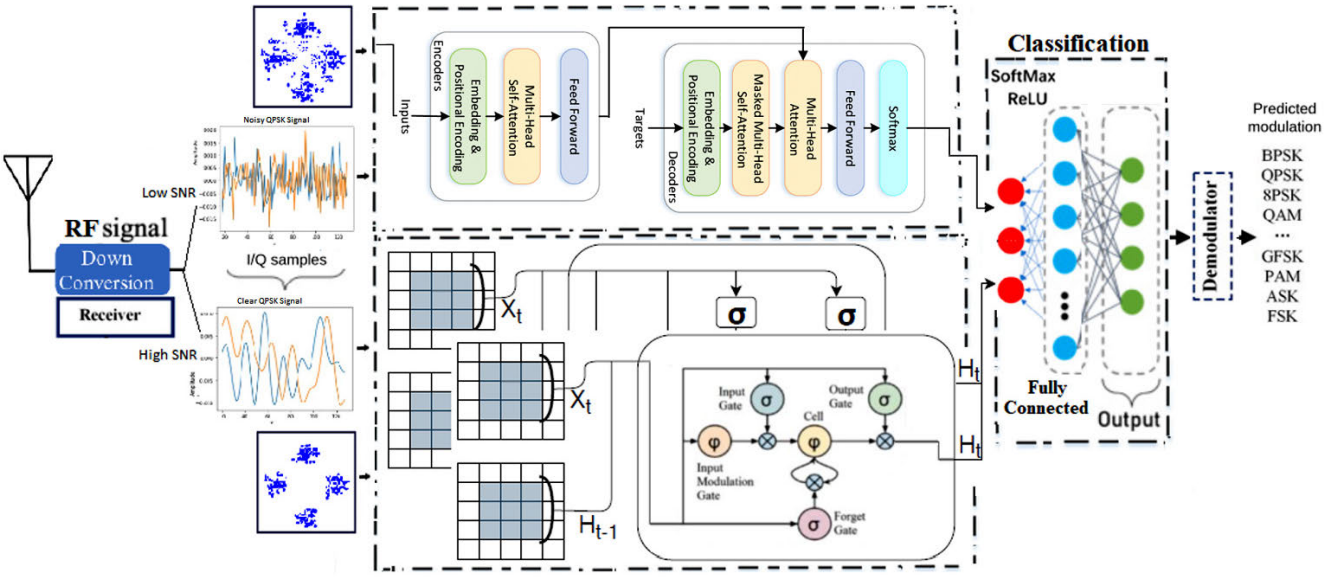


**FIGURE 8.** Proposed automatic modulation classification model using combinatorial deep learning technique for both low and high SNR signal classification.

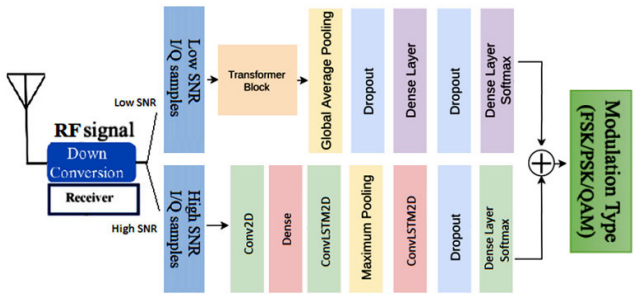


**FIGURE 9.** Proposed combinatorial deep learning classification model for both low SNR and high SNR modulation recognition.

weights are given by [2], [8], [43]

$$a = \text{softmax}\left(\frac{QK^T}{\sqrt{d_k}}\right). \tag{54}$$

It uses different transformations activation functions to transform the input and eliminates the need for recurrent connections [2], [8], [13], [43].

Our proposed model has advantage in using transformer-block network since it uses parallelization processing thus make use of parallel computation. In turn faster training time and inference testing time in using parallelization. Moreover, the input size can be any vector length and simultaneously proceed by the transformer-block encoder-decoder attention instead of sequentially hence solving the vanishing gradient problem. Also, context of data is well captured positional encoding and self-attention mechanism.

To increase the overall accuracy performance and to capture more context of the input data, a transformer-block network is implemented as a second stream in our proposed architecture as shown in Fig. 9. The layer type and output shape for the transformer-block network structure specific to each layer that is implemented is shown in Table 4. The proposed architecture consists of an input layer of $128 \times 2$ IQ input, followed by a Conv1D layer with 64 filters and 8 kernels then a MaxPooling1D layer and then a ConvLSTM and a Dropout layer follows with the same parameters. After that a Transformer-block and a *GlobalAveragePooling1D* followed by Dropout layer with the same parameters and a Dense and Dropout layer. At the end is a fully connected layer with an output size 11. Softmax is used as the activation function for multi-class classification. The Transformer uses a stochastic gradient descent (SGD) optimizer and starts with a learning rate of 0.03, which can be lowered during the training.

**TABLE 4.** Transformer-block network model layers.

| Layer type | Output Shape |
|---|---|
| Input | 128x2 |
| *Conv1D* | 121x64 |
| *MaxPooling1D* | 60x64 |
| *ConvLSTM* | 60x64 |
| *Dropout* | 60x64 |
| *Transformer_block* | 60x64 |
| *GlobalAveragePooling1D* | 64 |
| *Dropout* | 64 |
| *Dense* | 20 |
| *Dropout* | 20 |
| *Dense (Softmax)* | 11 |

## V. RML2016.10a and RML2016.10b RADIO SIGNAL DATASET

DeepSig radio signal datasets RadioML2016.10a [44] [45] and RadioML2016.10b [21] are used for evaluating the modulation recognition of our proposed models.

**TABLE 5. RadioML2016.10a DeepSig dataset parameters.**

| Parameter | VALUE |
|---|---|
| Modulations | 11 Classes, 8 digital, 3 analog modulations |
| Length per sample | 2x128 |
| *Signal format* | In-phase & Quadrature IQ |
| *Samples per symbol* | 8 |
| *Total number of samples* | 220,000 |
| *Sampling frequency* | 1 MHz |
| *SNR Range* | [-20:2:18]dB |
| *Training Samples* | 176,000 |
| *Test Samples* | 44,000 |

**TABLE 6. RadioML2016.10B DeepSig dataset parameters.**

| Parameter | VALUE |
|---|---|
| Modulations | 10 Classes, 8 digital, 2 analog |
| Length per sample | 2x128 |
| *Signal format* | In-phase & Quadrature IQ |
| *Signal dimension* | 2x128 per sample |
| *Total number of samples* | 1,200,000 |
| *Duration per sample* | 128 µs |
| *SNR Range* | [-20:2:18]dB |
| *Training Samples* | 960,000 |
| *Test Samples* | 240,000 |

The RML2016.10a dataset parameters [44] are shown in Table 5. It contains 220,000 samples, each represented using two vectors each of them has 128 elements Shape: (220,000, 2, 128) [46]. The IQ signal input component. A batch size of 128 is used on each training epoch [45].

The RML2016.10b dataset parameters [21] are shown in Table 6. It contains 1.2M samples, each represented using two vectors each of them has 128 elements Shape: (1200000, 2, 128) [46]. The IQ signal input component. A batch size of 128 is used on each training epoch.

The Nvidia Tesla A100 Tensor Core GPU is used to speed up the calculation. Models are implemented done using Keras framework with Nvidia A100 Tensor Core GPU.

The 128-sample baseband IQ time-domain signal data is used to identify the modulation type out of 11 modulations. based on power spectrum and time. The input data is fed in where the real and imaginary parts of samples are separated as shown in Fig. 10 and Fig. 11 [47].

Received r(t) signal is sampled into its discrete signal r[n], that is of the in-phase (I) components $r^I[n]$ and quadrature (Q) components $r^Q[n]$ are given as [36], [46], [48]

$$r[n] = r^I[n] + jr^Q[n]. \tag{55}$$

In reality the signal is always not ideal and combined with unwanted signal that is considered as noise which can affect

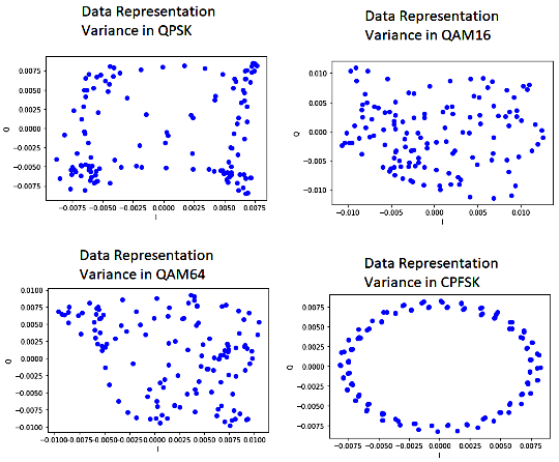


**FIGURE 10. IQ signal data samples constellation diagram where signals are represented by two vectors one for quadrature and other for In-phase representation.**

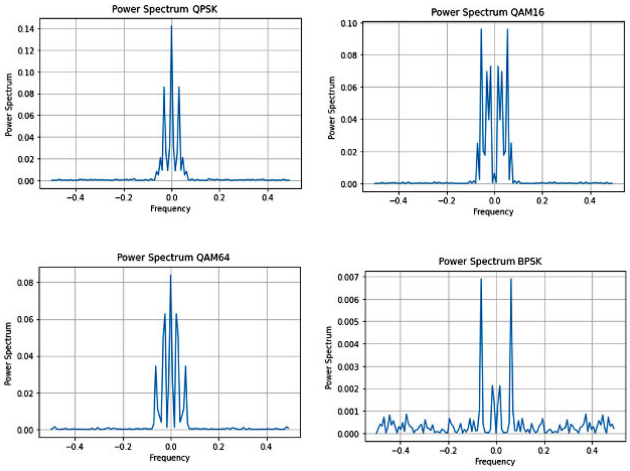


**FIGURE 11. IQ signal data samples power spectrum representation.**

our ability to determine the signal. Their relationship with the transmitter side I[n] and Q[n] is given by [36], [49], [50]

$$r^I[n] = I[n]\cos(2\pi fn + \varphi) - Q[n]\sin(2\pi fn + \varphi) + n_{add}[n]. \tag{56}$$

$$r^Q[n] = -I[n]\sin(2\pi fn + \varphi) - Q[n]\cos(2\pi fn + \varphi) + n_{add}[n]. \tag{57}$$

To construct the relation between $I$ and $Q$ components, the transformation function can be expressed as [36]

$$r[n] = radius[n] = \sqrt{I[n]^2 - Q[n]^2}. \tag{58}$$

$$\theta[n] = theta[n] = \arctan\left(\frac{I[n]}{Q[n]}\right). \tag{59}$$

We detect signals from their time representation showing value of each signal at a given time where each sample is represented by two vectors one for Quadrature and other for In-phase representation and the variance of data shown in

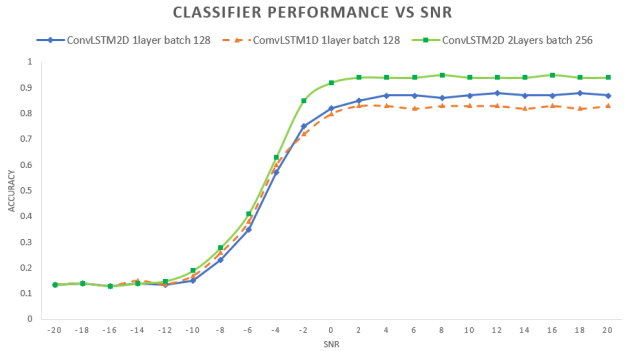


**FIGURE 12.** Classifier accuracy performance versus SNR for high SNR modulation recognition increase model layer with batch size.

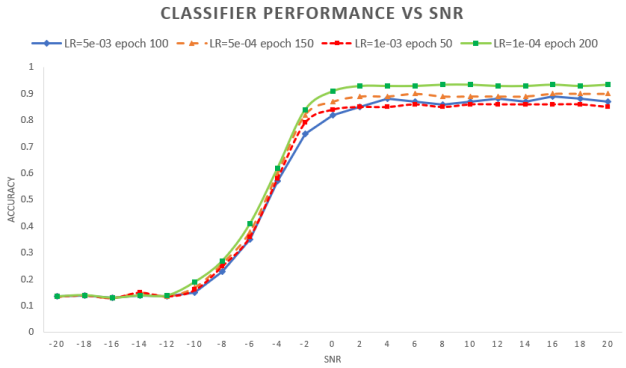


**FIGURE 13.** Varying learning rate and epoch with hyperparameter tunning.

Fig. 10 and Fig. 11. We should be able to classify signals both in low SNR and high SNR.

## VI. CLASSIFICATION PERFORMANCE SIMULATION RESULTS

The simulation results show that our proposed deep learning model is robust under noisy signal modulation without the need of denoising the noisy signal. The simulation results show our technique outperforms existing feature-based extraction architectures in terms of modulation recognition performance getting better accuracy in lower SNR signals without sacrifice accuracy in higher SNR signals.

Our proposed deep learning modulation classification technique achieves improved classification accuracy of 66% for low SNR signals and 93.5% at high SNR. As shown in Fig. 12, Fig. 13 and Fig. 14 overall classification accuracy against SNR.

The overall classification performance of our proposed deep learning model for high SNR signals is shown in Fig. 13. Two ConvLSTM2D layers gives better accuracy than one ConvLSTM2D layer with batch size of 256 achieving accuracy of 93.5% for High SNR signals.

The overall classification performance of our proposed deep learning model for high SNR signals is shown in Fig. 13. Tuning the learning rate hyperparameter to 0.0001 with

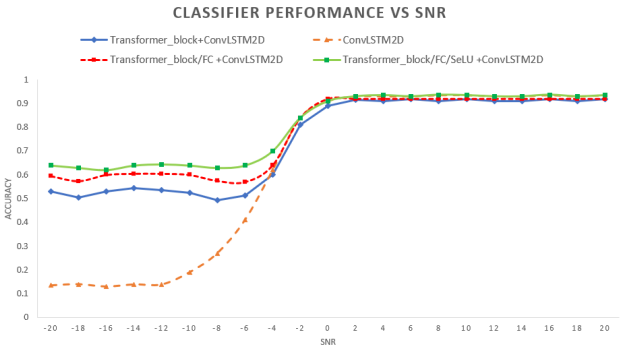


**FIGURE 14.** Combined transformer-block with ConvLSTM neural network SNR classifier performance.

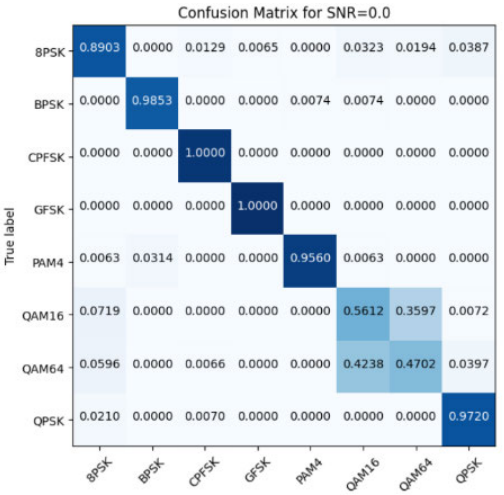


**FIGURE 15.** Confusion matrix of our proposed deep learning model for digital modulations at 0dB SNR with 50 epochs.

200 epochs gives higher classification accuracy achieving accuracy of 93.5% for High SNR signals.

As shown in Fig. 14 our proposed deep learning modulation classification technique achieves improved classification accuracy of 66% for low SNR signals and 93.5% at high SNR. Using our hybrid deep learning model by combining both ConvLSTM2D with Transformer-block neural networks, the proposed modulation classifier architecture can learn the signal for both low and high SNR and get better accuracy for signals with high noise. Showing that our model is robust under noisy signal modulation.

We analyze the classification accuracy of our proposed model for different modulation with DeepSig RadioML2016.10a dataset. The confusion matrix presents what modulation classes the model is confusing with other modulation classes. A dark blue along the diagonal represents a perfect classification.

The confusion matrix performance of the proposed deep learning model for digital modulation signals at 0dB SNR with 50 epochs is shown in Fig. 15. We analyze the classification accuracy of our proposed model for different modulation with DeepSig RadioML2016.10a dataset.

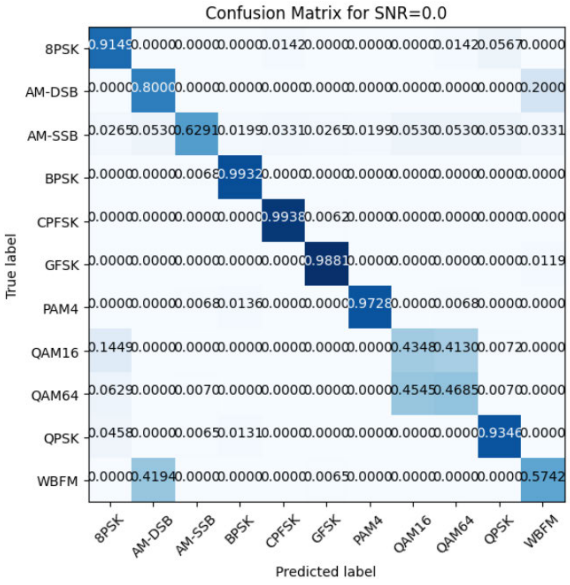


**FIGURE 16.** Confusion matrix of our proposed deep learning model for both digital and analog modulations at 0dB SNR with 300 epochs.

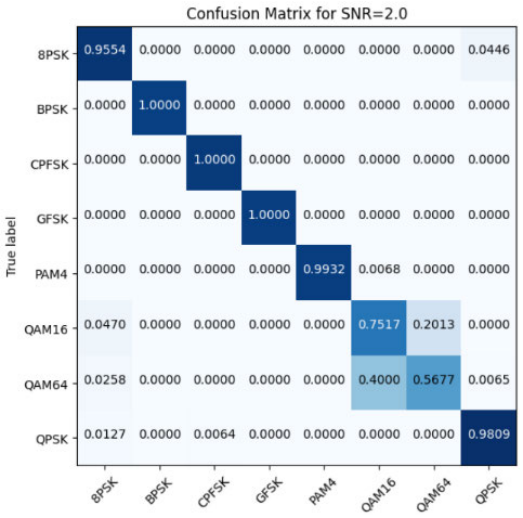


**FIGURE 17.** Confusion matrix of our proposed deep learning model for digital modulations at 2dB SNR with 50 epochs.

The confusion matrix performance of the proposed deep learning model for digital and analog modulation signals at 0dB SNR with 300 epochs is shown in Fig. 16. We analyze the classification accuracy of our proposed model for different modulation with DeepSig RadioML2016.10a dataset.

The confusion matrix performance of the proposed deep learning model for digital modulation signals at 2dB SNR with 50 epochs is shown in Fig. 17.

The confusion matrix performance of the proposed deep learning model for digital and analog modulation signals at 2dB SNR with 300 epochs is shown in Fig. 18.

The confusion matrix performance of the proposed deep learning model for digital modulation signals at −16dB SNR with 50 epochs is shown in Fig. 19.

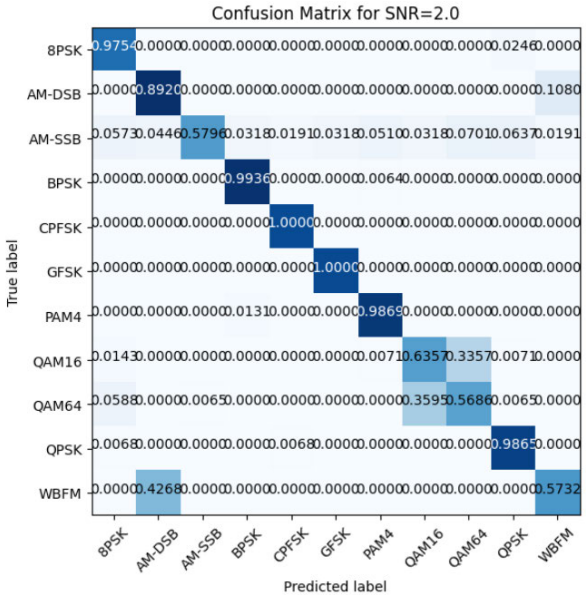


**FIGURE 18.** Confusion matrix of our proposed deep learning model for both digital and analog modulations at 2dB SNR with 300 epochs.

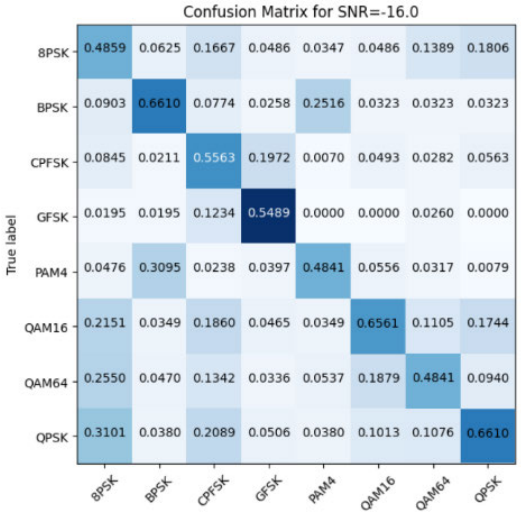


**FIGURE 19.** Confusion matrix of our proposed deep learning model for digital modulations at -16dB SNR with 50 epochs.

The confusion matrix performance of the proposed deep learning model for digital and analog modulation signals at −14dB SNR with 300 epochs is shown in Fig. 20.

The confusion matrix performance of the proposed deep learning model for digital modulation signals at 4dB SNR with 50 epochs is shown in Fig. 21.

The confusion matrix performance of the proposed deep learning model for digital and analog modulation signals at 4dB SNR with 300 epochs is shown in Fig. 22.

The confusion matrix performance of the proposed deep learning model for digital modulation signals at 6dB SNR with 50 epochs is shown in Fig. 23.

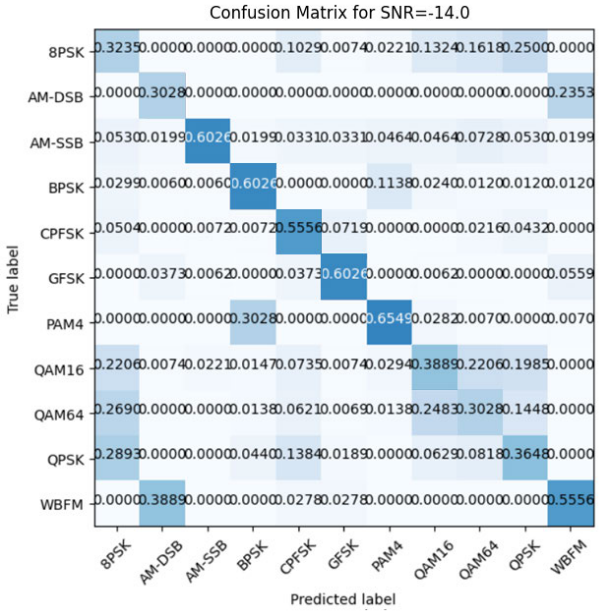


**FIGURE 20.** Confusion matrix of our proposed deep learning model for both digital and analog modulations at -14dB SNR with 300 epochs.

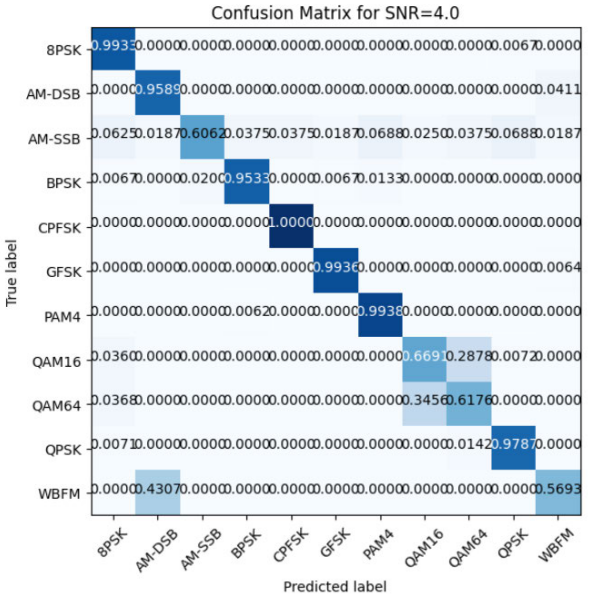


**FIGURE 22.** Confusion matrix of our proposed deep learning model for both digital and analog modulations at 4dB SNR with 300 epochs.

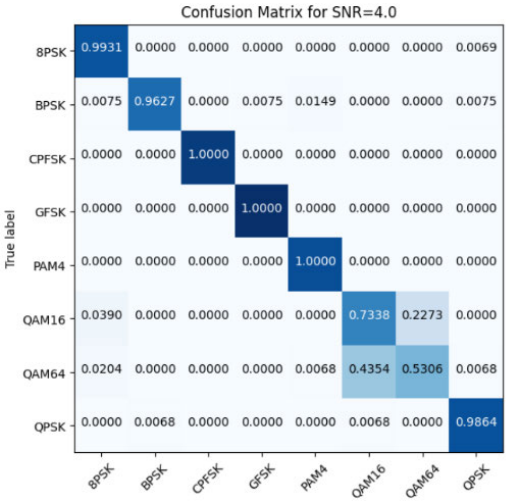


**FIGURE 21.** Confusion matrix of our proposed deep learning model for digital modulations at 4dB SNR with 50 epochs.

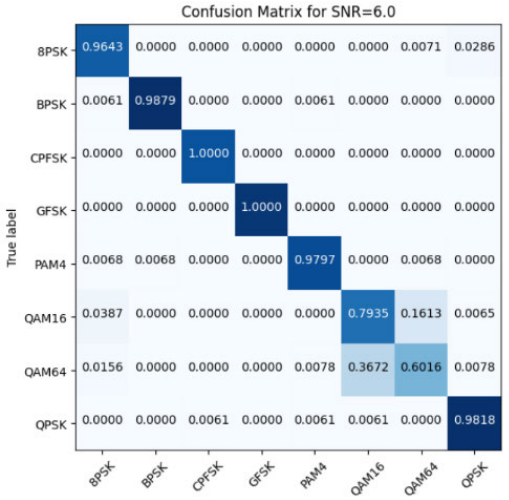


**FIGURE 23.** Confusion matrix of our proposed deep learning model for digital modulations at 6dB SNR with 50 epochs.

The confusion matrix performance of the proposed deep learning model for digital and analog modulation signals at 6dB SNR with 300 epochs is shown in Fig. 24.

The confusion matrix performance of the proposed deep learning model for digital modulation signals at 8dB SNR with 50 epochs is shown in Fig. 25.

The confusion matrix performance of the proposed deep learning model for digital and analog modulation signals at 8dB SNR with 300 epochs is shown in Fig. 26.

The confusion matrix performance of the proposed deep learning model for digital modulation signals at 10dB SNR with 50 epochs is shown in Fig. 27.

The confusion matrix performance of the proposed deep learning model for digital and analog modulation signals at 10dB SNR with 300 epochs is shown in Fig. 28.

The confusion matrix performance of the proposed deep learning mode for digital modulation signals at 12dB SNR with 50 epochs is shown in Fig. 29.

The confusion matrix performance of the proposed deep learning mode for digital and analog modulation signals at 12dB SNR with 300 epochs is shown in Fig. 30.

The confusion matrix performance of the proposed deep learning mode for digital modulation signals at 14dB SNR with 50 epochs is shown in Fig. 31.

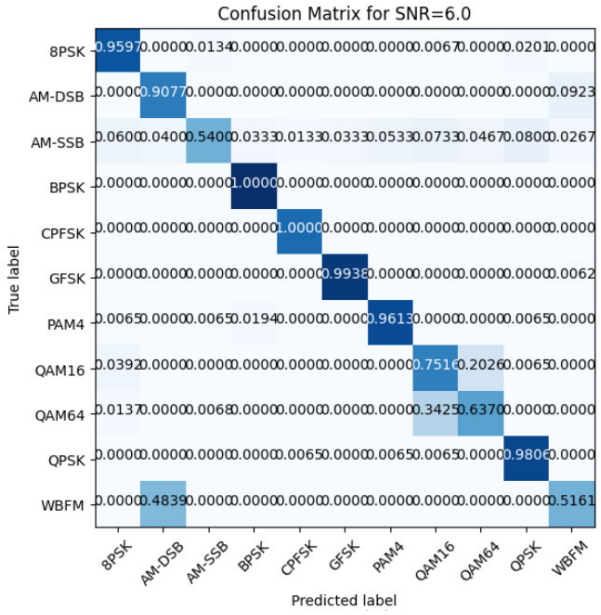


**FIGURE 24.** Confusion matrix of our proposed deep learning model for both digital and analog modulations at 6dB SNR with 300 epochs.

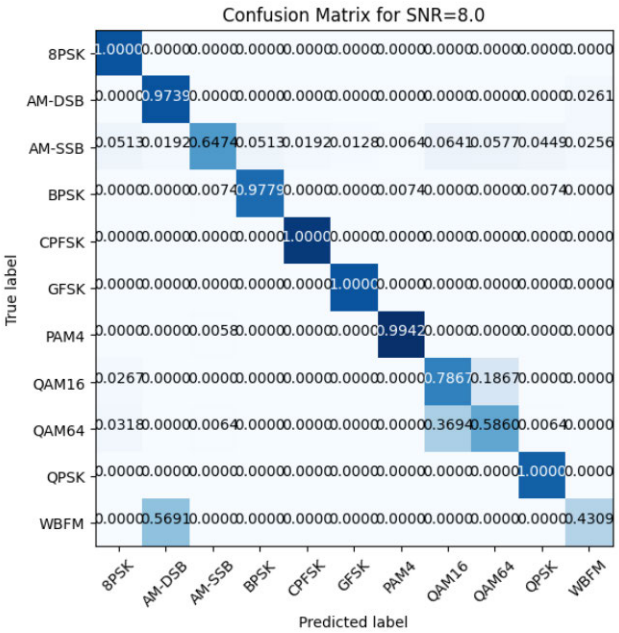


**FIGURE 26.** Confusion matrix of our proposed deep learning model for both digital and analog modulations at 8dB SNR with 300 epochs.

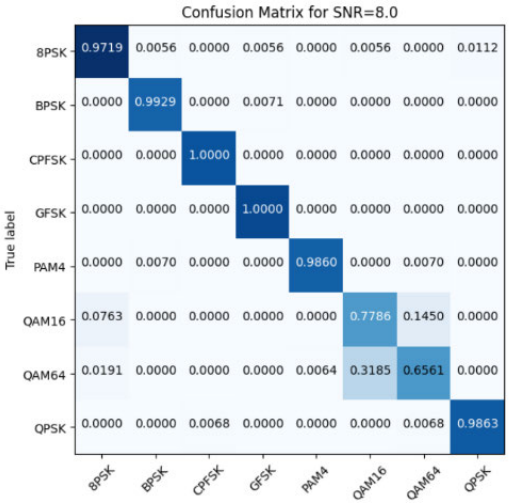


**FIGURE 25.** Confusion matrix of our proposed deep learning model for digital modulations at 8dB SNR with 50 epochs.

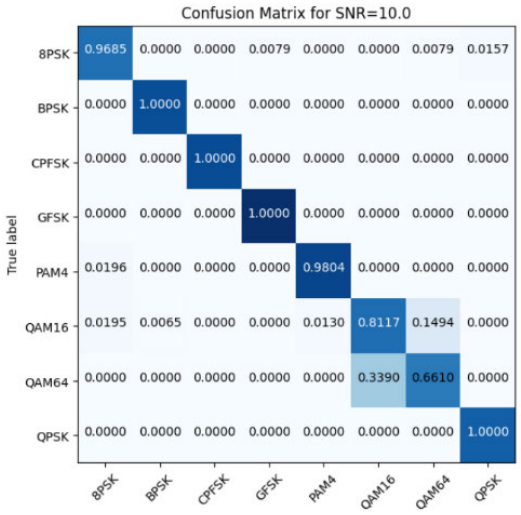


**FIGURE 27.** Confusion matrix of our proposed deep learning model for digital modulations at 10dB SNR with 50 epochs.

The confusion matrix performance of the proposed deep learning model for digital and analog modulation signals at 14dB SNR with 300 epochs is shown in Fig. 32.

The confusion matrix performance of the proposed deep learning mode for digital modulation signals at 16dB SNR with 50 epochs is shown in Fig. 33.

The confusion matrix performance of the proposed deep learning mode for digital and analog modulation signals at 16dB SNR with 300 epochs is shown in Fig. 34.

The confusion matrix performance of the proposed deep learning mode for signals at 18dB SNR with 50 epochs is shown in Fig. 35.

The confusion matrix performance of the proposed deep learning mode for digital and analog modulation signals at 18dB SNR with 300 epochs is shown in Fig. 36.

The results of the confusion matrix in Fig, 15 to Fig. 36 show that our proposed model performs well across most signal types as shown in the confusion matrix in Fig. 15 to Fig. 36. We analyze the classification accuracy of our proposed model for different modulation with DeepSig RadioML2016.10a dataset.

It is noted that QAM16 is often misrecognized as QAM64 and vice versa because the constellation points of QAM16 can be found in the constellation points of QAM64 so they can have constellation in common which causes short time observation to suffer. Moreover, features for a signal with

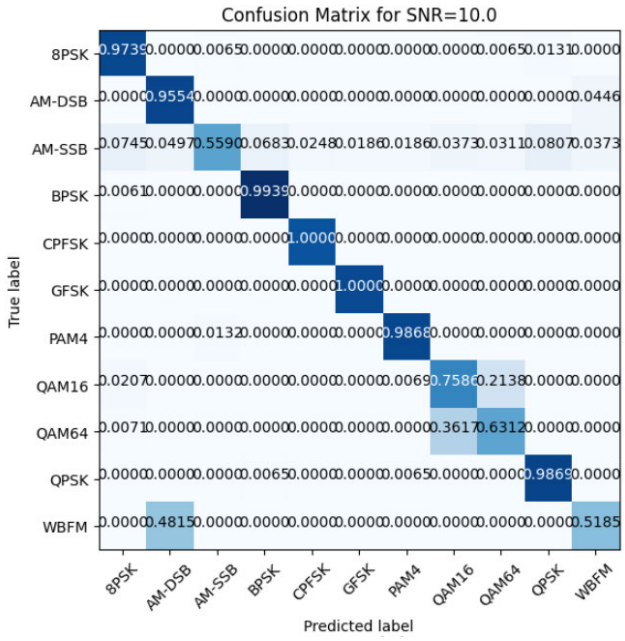


**FIGURE 28.** Confusion matrix of our proposed deep learning model for both digital and analog modulations at 10dB SNR with 300 epochs.

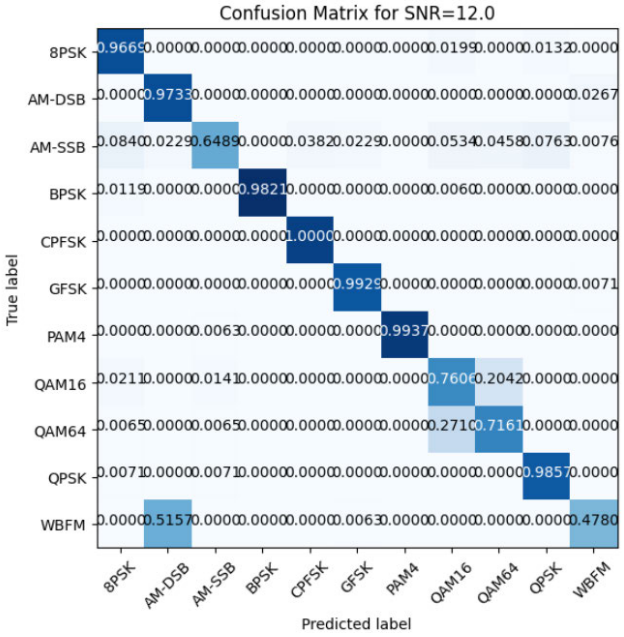


**FIGURE 30.** Confusion matrix of our proposed deep learning model for both digital and analog modulations at 12dB SNR with 300 epochs.

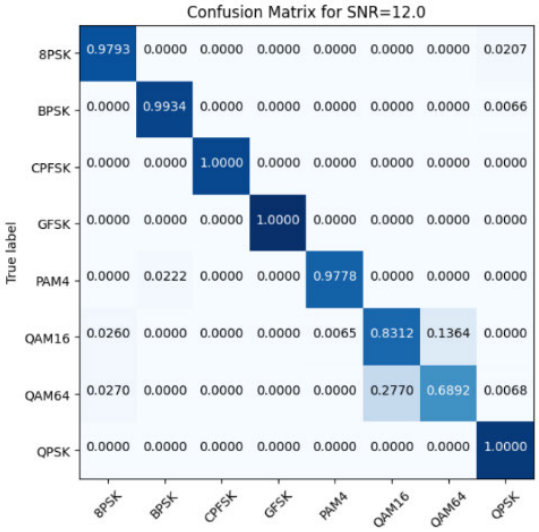


**FIGURE 29.** Confusion matrix of our proposed deep learning model for digital modulations at 12dB SNR with 50 epochs.

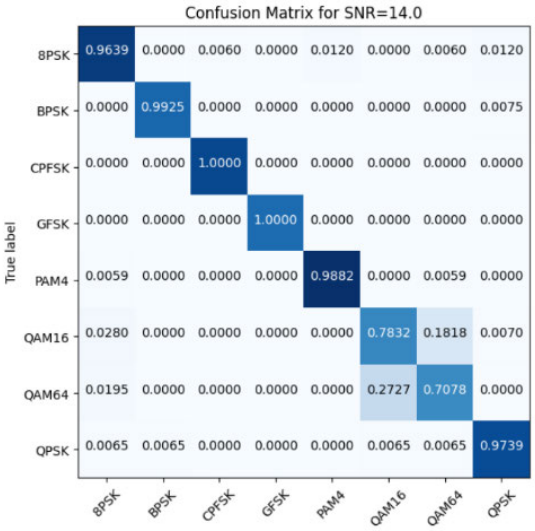


**FIGURE 31.** Confusion matrix of our proposed deep learning model for digital modulations at 14dB SNR with 50 epochs.

QAM64 modulation may not be captured by just 128 samples and so the deep network confuses it with QAM16 and therefore might benefit from a bigger dataset.

The accuracy performance of the proposed deep learning model per various modulation type versus SNR is shown in Fig. 37. A noisy signal will have a low SNR that means that if the noise is higher, the model will likely to less accuracy to do the modulation classification.

The overall classification performance of the proposed combined deep learning model is shown in Table 7.

The accuracy performance of the proposed deep learning model per various modulation type versus SNR from −20 dB to −2 dB is shown in Table 8.

**TABLE 7.** Overall classification performance.

| SNR | MODEL | Accuracy |
|---|---|---|
| High SNR Signals | ConvLSTM | 93.5% for High SNR Signals |
| Low SNR Signals | Transformer-block | 62% for Low SNR Signals |
| Both High and Low SNR Signals | Transformer-block + ConvLSTM | 62% for Low SNR and 93.5% for High SNR Signals |

The accuracy performance of the proposed deep learning model per various modulation type versus SNR from 0 dB to 20 dB is shown in Table 9.

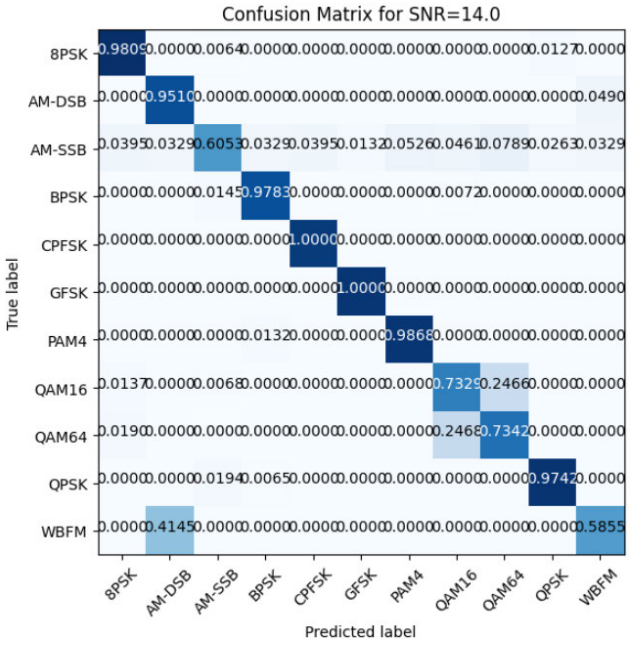


**FIGURE 32.** Confusion matrix of our proposed deep learning model for both digital and analog modulations at 14dB SNR with 300 epochs.

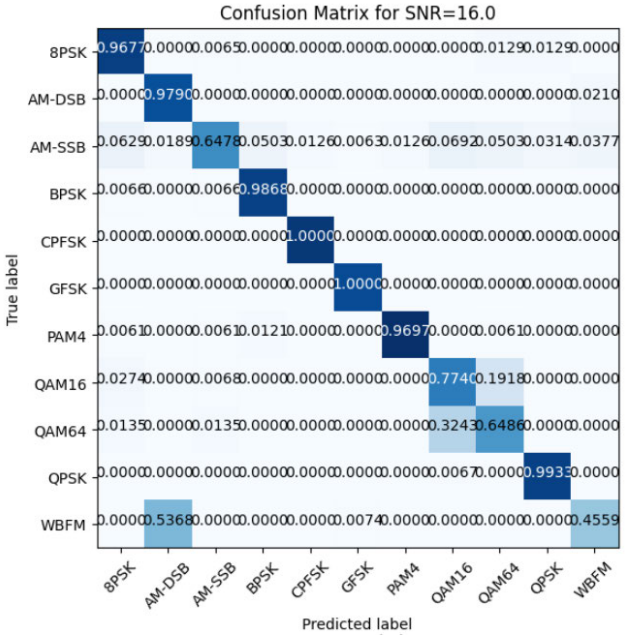


**FIGURE 34.** Confusion matrix of our proposed deep learning model for digital and analog modulations at 16dB SNR with 300 epochs.

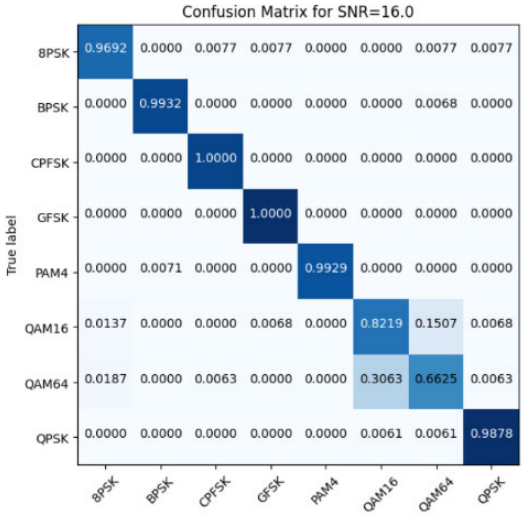


**FIGURE 33.** Confusion matrix of our proposed deep learning model for digital modulations at 16dB SNR with 50 epochs.

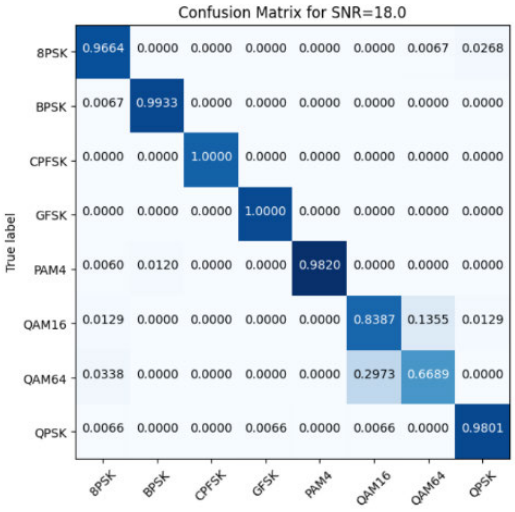


**FIGURE 35.** Confusion matrix of our proposed deep learning model for digital modulations at 18dB SNR with 50 epochs.

The overall training and prediction time performance of the proposed combined deep learning model compared to other models is shown in Table 10.

Other published work [25] that do not use deep learning models do not have the capability of applying automatic modulation recognition prediction. Other published work [44] that use deep learning models only achieve high accuracy in high SNR signals only unlike our proposed work where we achieve high accuracy in both high and low SNR signals. One of the main advantages of our proposed work is that our combined deep learning model provide the capability of loading automatic modulation recognition on hardware accelerator chips to take processing load of the main hardware processor. Also, another advantage of our proposed work is that by utilizing Transformer-block processing utilized for larger training data set parallelization in our combined model resulting in faster training time and inference testing as shown in Table 10. However, does not achieve the fastest prediction and training time compared combined models which is one of the shortcomings of our combined deep learning model.

As can be seen in Fig. 38, X. Hao [18] used CLDNN+ GRU model achieving accuracy of 90% at 0 dB SNR and less than 20% at −16 dB SNR. S. Huang [4] used Comprehensive CNN model achieving accuracy of 80% at 0 dB SNR and less than 20% at −16 dB SNR. X. Xie [35] used DenseNet and BLSTM model achieving accuracy of 84% at 0 dB SNR and less than 25% at −16 dB SNR. H. Yang [21] used IRLNet model achieving accuracy of 97% at 5 dB SNR and less

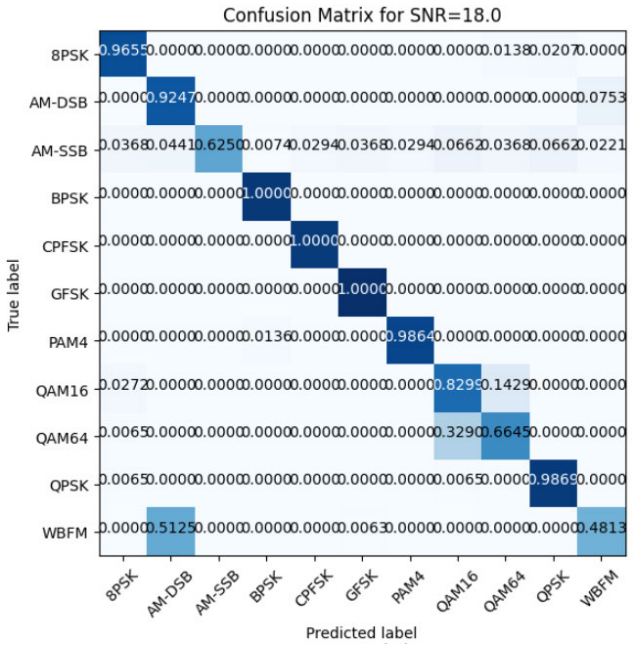


**FIGURE 36.** Confusion matrix of our proposed deep learning model for digital and analog modulations at 16dB SNR with 300 epochs.

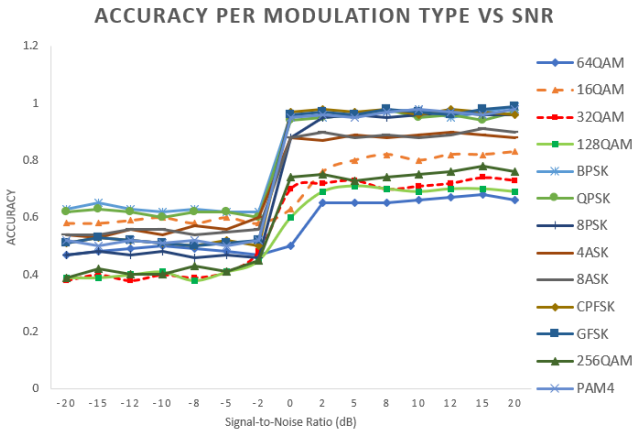


**FIGURE 37.** Accuracy performance of the proposed deep learning model per various modulation type versus SNR.

**TABLE 8.** Accuracy performance per various modulation type versus SNR.

| Modulation Type | -20 | -15 | -12 | -10 | -8 | -5 | -2 |
|---|---|---|---|---|---|---|---|
| 16QAM | 0.58 | 0.58 | 0.59 | 0.60 | 0.58 | 0.60 | 0.58 |
| 32QAM | 0.40 | 0.41 | 0.39 | 0.40 | 0.39 | 0.41 | 0.48 |
| 64QAM | 0.47 | 0.47 | 0.49 | 0.50 | 0.49 | 0.48 | 0.47 |
| 128QAM | 0.41 | 0.40 | 0.40 | 0.41 | 0.38 | 0.41 | 0.45 |
| 256QAM | 0.41 | 0.42 | 0.40 | 0.40 | 0.43 | 0.41 | 0.45 |
| BPSK | 0.63 | 0.65 | 0.63 | 0.62 | 0.63 | 0.62 | 0.62 |
| QPSK | 0.62 | 0.63 | 0.62 | 0.60 | 0.62 | 0.62 | 0.60 |
| 8PSK | 0.47 | 0.48 | 0.47 | 0.48 | 0.46 | 0.47 | 0.46 |
| 4ASK | 0.54 | 0.53 | 0.56 | 0.54 | 0.57 | 0.54 | 0.60 |
| 8ASK | 0.54 | 0.54 | 0.56 | 0.56 | 0.54 | 0.55 | 0.56 |
| PAM4 | 0.52 | 0.51 | 0.52 | 0.51 | 0.52 | 0.50 | 0.52 |
| CPFSK | 0.51 | 0.53 | 0.52 | 0.51 | 0.50 | 0.52 | 0.50 |
| GFSK | 0.51 | 0.53 | 0.52 | 0.51 | 0.50 | 0.51 | 0.52 |

than 50% at −16 dB SNR. F. Liu [32] used GRU model achieving accuracy of 86% at 0 dB SNR and less than 55%

**TABLE 9.** Accuracy performance per various modulation type versus SNR.

| Modulation Type | 0 | 2 | 5 | 8 | 10 | 15 | 20 |
|---|---|---|---|---|---|---|---|
| 16QAM | 0.63 | 0.76 | 0.80 | 0.82 | 0.66 | 0.82 | 0.83 |
| 32QAM | 0.70 | 0.72 | 0.73 | 0.70 | 0.71 | 0.74 | 0.73 |
| 64QAM | 0.50 | 0.65 | 0.65 | 0.65 | 0.66 | 0.68 | 0.66 |
| 128QAM | 0.60 | 0.69 | 0.71 | 0.70 | 0.69 | 0.70 | 0.70 |
| 256QAM | 0.74 | 0.75 | 0.73 | 0.74 | 0.75 | 0.78 | 0.76 |
| BPSK | 0.96 | 0.95 | 0.96 | 0.97 | 0.98 | 0.97 | 0.99 |
| QPSK | 0.94 | 0.95 | 0.96 | 0.98 | 0.95 | 0.94 | 0.97 |
| 8PSK | 0.88 | 0.95 | 0.96 | 0.95 | 0.96 | 0.96 | 0.96 |
| 4ASK | 0.88 | 0.87 | 0.89 | 0.88 | 0.89 | 0.89 | 0.88 |
| 8ASK | 0.88 | 0.90 | 0.88 | 0.89 | 0.88 | 0.91 | 0.90 |
| PAM4 | 0.95 | 0.96 | 0.95 | 0.97 | 0.98 | 0.96 | 0.98 |
| CPFSK | 0.97 | 0.98 | 0.97 | 0.98 | 0.96 | 0.97 | 0.96 |
| GFSK | 0.96 | 0.97 | 0.96 | 0.98 | 0.97 | 0.98 | 0.99 |

**TABLE 10.** Overall training & prediction time performance.

| Model | Training Time Per Epoch (s) | Prediction Time (μ/sample) | Training Time (s) |
|---|---|---|---|
| CNN [44] | 30 | 1000 | 600 |
| LSTM [44] | 800 | 2000 | 44800 |
| SCRNN [44] | 280 | 600 | 11480 |
| ResNet [51] | 341 | 183 | 1850 |
| Transformer-block + ConvLSTM (this work) | 320 | 730 | 2250 |

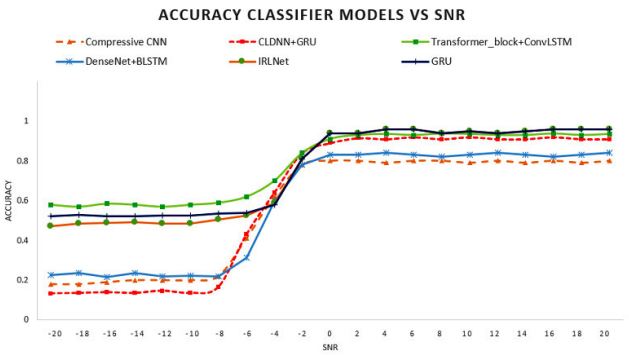


**FIGURE 38.** Accuracy performance of the proposed deep learning model per various Models type versus SNR.

at −16 dB SNR. Our proposed model used ConvLSTM and Transformer-block model achieving accuracy of 93.5% at 0 dB SNR and 62% at −16 dB SNR.

As shown in Table 11, our proposed model used ConvLSTM and Transformer-block model achieving accuracy of 93.5% at 0 dB SNR and 62% at −16 dB SNR. Whereas F. Liu [32] used GRU model achieving accuracy of 86% at 0 dB SNR and less than 55% at −16 dB SNR. H. Yang [21] used IRLNet model achieving accuracy of 97% at 5 dB SNR and less than 50% at −16 dB SNR. X. Xie [35] used DenseNet and BLSTM model achieving accuracy of 84% at 0 dB SNR

**TABLE 11. Overall classification modulation recognition accuracy performance comparison.**

| Author | Input Signal | Model | Recognition Accuracy |
|---|---|---|---|
| K. Jiang [12] | IQ sequence | CNN + Bi LSTM | 90% (0 dB) & < 10% (-16 dB) |
| B. Tang [10] | constellation map | CNN + GAN | 100% (-2 dB) & < 10% (-16 dB) |
| J. Xu [11] | IQ sequence | CNN + LSTM + FC | 90% (0 dB) & < 10% (-16 dB) |
| Z. Liang [13] | IQ sequence | ResNeXt + Attention | 90% (0 dB) & < 10% (-16 dB) |
| W. Zhang[15] | Sampled signal | GRU + CNN | 99.45% (0 dB) & < 10% (-16 dB) |
| S. Chang [14] | Sampled signal | CNN + Bi GRU + SAFN | 84% (0 dB) & <10% (-16 dB) |
| B. Liu [20] | IQ sequence | DCN + Bi LSTM | 90% (0 dB) & < 10% (-16 dB) |
| J. Bai [17] | IQ sequence | DMFF + CNN | 90% (0 dB) & < 10% (-16 dB) |
| B. Udaya [19] | IQ sequence | LSTM + Bi LSTM | 90% (0 dB) & < 10% (-16 dB) |
| B. Zou [16] | IQ sequence | Attention + CLDNN | 90% (4 dB) & < 10% (-16 dB) |
| X. Hao [18] | IQ sequence | CLDNN+GRU | 90% (0 dB) & <20% (-16 dB) |
| S. Huang [4] | IQ sequence | Compressive CNN | 80% (0 dB) & <20% (-16 dB) |
| X. Xie [35] | IQ sequence | DenseNet-BLSTM | 84% (0 dB) & <25% (-16 dB) |
| H. Yang [21] | IQ sequence | IRLNET | 97% (5 dB) & <50% (-16 dB) |
| F. Liu [32] | IQ sequence | GRU | 86% (0 dB) & <55% (-16 dB) |
| (This work) | IQ sequence | Transformer-block + ConvLSTM | 93.5% (0 dB) & 62% (-16 dB) |

and less than 25% at −16 dB SNR. And S. Huang [4] used Comprehensive CNN model achieving accuracy of 80% at 0 dB SNR and less than 20% at −16 dB SNR. And X. Hao [18] used CLDNN+GRU model achieving accuracy of 90% at 0 dB SNR and less than 20% at −16 dB SNR. All other published models in Table 11 achieve less than 10% at −16 dB SNR compared to our proposed model.

We compare our proposed models in terms of the number of trainable parameters, the number of floating point operations (FLOPs) and the memory cost as shown in Table 12. Smaller number of trainable parameters requires fewer FLOPs and the smaller memory space.

It can be seen in Table 12 that our proposed model needs to train 1702625 parameters with total number of 60662829 floating point operations (FLOPs) at a 19.7MB memory cost. Whereas LTSM model in [1] needs to train 199563 parameters with total number of 7696283 floating point operations (FLOPs) at a 2.31MB memory cost. Also, CNN [1] needs to train 5456219 parameters with total number of 80548043 floating point operations (FLOPs) at a 61.4MB memory cost as shown in Table 12.

**TABLE 12. Model layer number of parameter.**

| Model Layer | Trainable Parameter | Number of Flops | Memory |
|---|---|---|---|
| CNN [23] | 5456219 | 80548043 | 61.4MB |
| LSTM [23] | 199563 | 7696283 | 2.31MB |
| This work | 1702625 | 60662829 | 19.7MB |

## VII. CONCLUSION

An automatic signal modulation classification model using combinatorial deep learning technique was presented. Our proposed deep learning model increase accuracy for low signal to noise ratio SNR and maintain a high classification accuracy for high SNR signals. Using a hybrid deep learning model combining both ConvLSTM2D with Transformer-block neural networks, the proposed modulation classifier architecture can learn the signal for both low and high SNR and get better accuracy for signals with high noise. The proposed deep learning modulation classification technique achieves improved classification accuracy of 66% for low SNR signals and 93.5% at high SNR showing that our model is robust under noisy signal modulation. Our deep learning radio modulation classification model works using raw signal without the need of denoising the noisy signal. The simulation results show that the proposed technique outperforms existing feature-based extraction architectures in terms of modulation recognition performance getting better accuracy in lower SNR signals without sacrifice accuracy in higher SNR signals.

## ACKNOWLEDGMENT

The authors would like to thank all who contributed to the research funding.

## REFERENCES

[1] W. Max Lees, A. Wunderlich, P. Jeavons, P. D. Hale, and M. R. Souryal, "Deep learning classification of 3.5 GHz band spectrograms with applications to spectrum sensing," 2018, *arXiv:1806.07745*.

[2] A. Vaswani, N. Shazeer, N. Parmar, J. Uszkoreit, L. Jones, A. N. Gomez, L. Kaiser, and I. Polosukhin, "Attention is all you need," 2017, *arXiv:1706.03762*.

[3] V. Sathyanarayanan, J. Burke, R. Shang, and R. Bell, "Modulation classification using neural networks," Noise Lab UCSD, Univ. California San Diego, San Diego, CA, USA, Tech. Rep. 42, 2019.

[4] S. Huang, L. Chai, Z. Li, D. Zhang, Y. Yao, Y. Zhang, and Z. Feng, "Automatic modulation classification using compressive convolutional neural network," *IEEE Access*, vol. 7, pp. 79636–79643, 2019, doi: 10.1109/ACCESS.2019.2921988.

[5] Y. Guo and X. Wang, "Modulation signal classification algorithm based on denoising residual convolutional neural network," *IEEE Access*, vol. 10, pp. 121733–121740, 2022, doi: 10.1109/ACCESS.2022.3221475.

[6] W.-T. Zhang, D. Cui, and S.-T. Lou, "Training images generation for CNN based automatic modulation classification," *IEEE Access*, vol. 9, pp. 62916–62925, 2021, doi: 10.1109/ACCESS.2021.3073845.

[7] N. E West and T. J. O'Shea, "Deep architectures for modulation recognition," 2017, *arXiv:1703.09197*.

[8] S. Chen, Y. Zhang, Z. He, J. Nie, and W. Zhang, "A novel attention cooperative framework for automatic modulation recognition," *IEEE Access*, vol. 8, pp. 15673–15686, 2020, doi: 10.1109/ACCESS.2020.2966777.

[9] J. Jiang, Z. Wang, H. Zhao, S. Qiu, and J. Li, "Modulation recognition method of satellite communication based on CLDNN model," in *Proc. IEEE 30th Int. Symp. on Indust. Elect.*, Jun. 2021, pp. 1–6, doi: 10.1109/ISIE45552.2021.9576379.

[10] B. Tang, Y. Tu, Z. Zhang, and Y. Lin, "Digital signal modulation classification with data augmentation using generative adversarial nets in cognitive radio networks," *IEEE Access*, vol. 6, pp. 15713–15722, 2018, doi: 10.1109/ACCESS.2018.2815741.

[11] J. Xu, C. Luo, G. Parr, and Y. Luo, "A spatiotemporal multi-channel learning framework for automatic modulation recognition," *IEEE Wireless Commun. Lett.*, vol. 9, no. 10, pp. 1629–1632, Oct. 2020, doi: 10.1109/LWC.2020.2999453.

[12] K. Jiang, X. Qin, J. Zhang, and A. Wang, "Modulation recognition of communication signal based on convolutional neural network," *Symmetry*, vol. 13, no. 12, p. 2302, Dec. 2021, doi: 10.3390/sym13122302.

[13] Z. Liang, M. Tao, L. Wang, J. Su, and X. Yang, "Automatic modulation recognition based on adaptive attention mechanism and ResNeXt WSL model," *IEEE Commun. Lett.*, vol. 25, no. 9, pp. 2953–2957, Sep. 2021, doi: 10.1109/LCOMM.2021.3093485.

[14] S. Chang, S. Huang, R. Zhang, Z. Feng, and L. Liu, "Multitask-learning-based deep neural network for automatic modulation classification," *IEEE Internet Things J.*, vol. 9, no. 3, pp. 2192–2206, Feb. 2022, doi: 10.1109/JIOT.2021.3091523.

[15] W. Zhang, X. Yang, C. Leng, J. Wang, and S. Mao, "Modulation recognition of underwater acoustic signals using deep hybrid neural networks," *IEEE Trans. Wireless Commun.*, vol. 21, no. 8, pp. 5977–5988, Aug. 2022, doi: 10.1109/TWC.2022.3144608.

[16] B. Zou, X. Zeng, and F. Wang, "Research on modulation signal recognition based on CLDNN network," *Electronics*, vol. 11, no. 9, p. 1379, Apr. 2022, doi: 10.3390/electronics11091379.

[17] J. Bai, J. Yao, J. Qi, and L. Wang, "Electromagnetic modulation signal classification using dual-modal feature fusion CNN," *Entropy*, vol. 24, no. 5, p. 700, May 2022, doi: 10.3390/e24050700.

[18] X. Hao, Y. Luo, Q. Ye, Q. He, G. Yang, and C.-C. Chen, "Automatic modulation recognition method based on hybrid model of convolutional neural networks and gated recurrent units," *Sensors Mater.*, vol. 33, no. 12, p. 4229, 2021, doi: 10.18494/sam.2021.3456.

[19] U. Dampage, S. M. R. P. Amarasooriya, R. A. S. M. Samarasinghe, and N. A. Karunasingha, "Combined classifier-demodulator scheme based on LSTM architecture," *Wireless Commun. Mobile Comput.*, vol. 2022, pp. 1–9, Jun. 2022, doi: 10.1155/2022/5584481.

[20] K. Liu, W. Gao, and Q. Huang, "Automatic modulation recognition based on a DCN-BiLSTM network," *Sensors*, vol. 21, no. 5, p. 1577, Feb. 2021, doi: 10.3390/s21051577.

[21] H. Yang, L. Zhao, G. Yue, B. Ma, and W. Li, "IRLNet: A short-time and robust architecture for automatic modulation recognition," *IEEE Access*, vol. 9, pp. 143661–143676, 2021, doi: 10.1109/ACCESS.2021.3121762.

[22] V. N. S. Kumaran, "Ensemble of deep learning enabled modulation signal classification model for underwater acoustic communication," SSRN, S.R.M. Inst. Sci. Technol., Tiruchirappalli, India, Tech. Rep., Jan. 2022. [Online]. Available: https://ssrn.com/abstract=4057312, doi: 10.2139/ssrn.4057312.

[23] Z. Ke and H. Vikalo, "Real-time radio technology and modulation classification via an LSTM auto-encoder," 2020, *arXiv:2011.08295*.

[24] C. Zhang, S. Yu, G. Li, and Y. Xu, "The recognition method of MQAM signals based on BP neural network and bird swarm algorithm," *IEEE Access*, vol. 9, pp. 36078–36086, 2021, doi: 10.1109/ACCESS.2021.3061585.

[25] T. K. Oikonomou, S. A. Tegos, D. Tyrovolas, P. D. Diamantoulakis, and G. K. Karagiannidis, "On the error analysis of hexagonal-QAM constellations," *IEEE Commun. Lett.*, vol. 26, no. 8, pp. 1764–1768, Aug. 2022, doi: 10.1109/LCOMM.2022.3179454.

[26] T. Wang, G. Yang, P. Chen, Z. Xu, M. Jiang, and Q. Ye, "A survey of applications of deep learning in radio signal modulation recognition," *Appl. Sci.*, vol. 12, no. 23, p. 12052, Nov. 2022, doi: 10.3390/app122312052.

[27] F. Shi, Z. Hu, C. Yue, and Z. Shen, "Combining neural networks for modulation recognition," *Digit. Signal Process.*, vol. 120, Jan. 2022, Art. no. 103264, doi: 10.1016/j.dsp.2021.103264.

[28] U. Madhow, *Introduction To Communication Systems*. Cambridge, U.K.: Cambridge Univ. Press, 2014.

[29] D. T. Kawamoto and R. W. Mcgwier, "Rigorous moment-based automatic modulation classification," in *Proc. GNU Radio Conf.*, Sep. 2016, pp. 1–11.

[30] C.-F. Teng, C.-C. Liao, C.-H. Chen, and A.-Y. Wu, "Polar feature based deep architectures for automatic modulation classification considering channel fading," *IEEE Global Conf. Signal Inf. Process. (GlobalSIP)*, Nov. 2018, pp. 554–558.

[31] Z. Wu, S. Zhou, Z. Yin, B. Ma, and Z. Yang, "Robust automatic modulation classification under varying noise conditions," *IEEE Access*, vol. 5, pp. 19733–19741, 2017, doi: 10.1109/ACCESS.2017.2746140.

[32] F. Liu, Z. Zhang, and R. Zhou, "Automatic modulation recognition based on CNN and GRU," *Tsinghua Sci. Technol.*, vol. 27, no. 2, pp. 422–431, Apr. 2022, doi: 10.26599/TST.2020.9010057.

[33] X. Hao, Z. Xia, M. Jiang, Q. Ye, and G. Yang, "Radio signal modulation recognition method based on deep learning model pruning," *Appl. Sci.*, vol. 12, no. 19, p. 9894, Oct. 2022, doi: 10.3390/app12199894.

[34] G. Wang, B. Li, T. Zhang, and S. Zhang, "A network combining a transformer and a convolutional neural network for remote sensing image change detection," *Remote Sens.*, vol. 14, no. 9, p. 2228, May 2022, doi: 10.3390/rs14092228.

[35] X. Xie, G. Yang, M. Jiang, Q. Ye, and C.-F. Yang, "A kind of wireless modulation recognition method based on DenseNet and BLSTM," *IEEE Access*, vol. 9, pp. 125706–125713, 2021, doi: 10.1109/ACCESS.2021.3111406.

[36] N. Wang, Y. Liu, L. Ma, Y. Yang, and H. Wang, "Multidimensional CNN-LSTM network for automatic modulation classification," *Electronics*, vol. 10, no. 14, p. 1649, Jul. 2021, doi: 10.3390/electronics10141649.

[37] W.-S. Hu, H.-C. Li, L. Pan, W. Li, R. Tao, and Q. Du, "Spatial–spectral feature extraction via deep ConvLSTM neural networks for hyperspectral image classification," *IEEE Trans. Geosci. Remote Sens.*, vol. 58, no. 6, pp. 4237–4250, Jun. 2020, doi: 10.1109/TGRS.2019.2961947.

[38] R. Zhou, F. Liu, and C. W. Gravelle, "Deep learning for modulation recognition: A survey with a demonstration," *IEEE Access*, vol. 8, pp. 67366–67376, 2020, doi: 10.1109/ACCESS.2020.2986330.

[39] V. Sathyanarayanan, J. Burke, R. Shang, and R. Bell, "Modulation classification using neural networks," Tech. Rep.

[40] K. Jiang, J. Zhang, H. Wu, A. Wang, and Y. Iwahori, "A novel digital modulation recognition algorithm based on deep convolutional neural network," *Appl. Sci.*, vol. 10, no. 3, p. 1166, Feb. 2020, doi: 10.3390/app10031166.

[41] L. Li, C. Qin, G. Li, S. Hu, Y. Xie, and Z. Lei, "Transformer-based radio modulation mode recognition," *J. Phys., Conf. Ser.*, vol. 2384, no. 1, Dec. 2022, Art. no. 012017, doi: 10.1088/1742-6596/2384/1/012017.

[42] Y. Zheng, Y. Ma, and C. Tian, "TMRN-GLU: A transformer-based automatic classification recognition network improved by gate linear unit," *Electronics*, vol. 11, no. 10, p. 1554, May 2022, doi: 10.3390/electronics11101554.

[43] F. Tian, L. Wang, and M. Xia, "Signals recognition by CNN based on attention mechanism," *Electronics*, vol. 11, no. 13, p. 2100, Jul. 2022, doi: 10.3390/electronics11132100.

[44] K. Liao, Y. Zhao, J. Gu, Y. Zhang, and Y. Zhong, "Sequential convolutional recurrent neural networks for fast automatic modulation classification," *IEEE Access*, vol. 9, pp. 27182–27188, 2021, doi: 10.1109/ACCESS.2021.3053427.

[45] T. Huynh-The, Q.-V. Pham, T.-V. Nguyen, T. T. Nguyen, R. Ruby, M. Zeng, and D.-S. Kim, "Automatic modulation classification: A deep architecture survey," *IEEE Access*, vol. 9, pp. 142950–142971, 2021, doi: 10.1109/ACCESS.2021.3120419.

[46] O. S. Mossad, M. ElNainay, and M. Torki, "Deep convolutional neural network with multi-task learning scheme for modulations recognition," in *Proc. 15th Int. Wireless Commun. Mobile Comput. Conf. (IWCMC)*, Jun. 2019, pp. 1644–1649, doi: 10.1109/IWCMC.2019.8766665.

[47] F. Zhang, C. Luo, J. Xu, Y. Luo, and F. Zheng, "Deep learning based automatic modulation recognition: Models, datasets, and challenges," 2022, *arXiv:2207.09647*.

[48] H. Han, Z. Ren, L. Li, and Z. Zhu, "Automatic modulation classification based on deep feature fusion for high noise level and large dynamic input," *Sensors*, vol. 21, no. 6, p. 2117, Mar. 2021, doi: 10.3390/s21062117.

[49] S. Ansari, K. A. Alnajjar, M. Saad, S. Abdallah, and A. A. El-Moursy, "Automatic digital modulation recognition based on genetic-algorithm-optimized machine learning models," *IEEE Access*, vol. 10, pp. 50265–50277, 2022, doi: 10.1109/ACCESS.2022.3171909.
[50] A. Jagannath and J. Jagannath, "Multi-task learning approach for automatic modulation and wireless signal classification," 2021, *arXiv:2101.10254*.
[51] M. M. Elsagheer and S. M. Ramzy, "A hybrid model for automatic modulation classification based on residual neural networks and long short term memory," *Alexandria Eng. J.*, vol. 67, pp. 117–128, Mar. 2023, doi: 10.1016/j.aej.2022.08.019.

**ZIAD ELKHATIB** (Member, IEEE) received the B.A.Sc. degree in electrical engineering from the University of Ottawa, Canada, and the M.A.Sc. and Ph.D. degrees in electrical and computer engineering from Carleton University, Canada. He was an Assistant Professor with the Faculty of Electrical and Computer Engineering, Rochester Institute of Technology Dubai. He is currently an Assistant Professor with the Faculty of Electrical and Computer Engineering, Canadian University Dubai. He has several years of industry design experience in the field of communication integrated circuits and semiconductors at various companies, including Nortel Networks, Harris Corporation, Corel Corporation, Chrysalis-ITS Semiconductor, and Itron Inc., USA, where he was an Adjunct Professor. He has a book published through Springer on radio frequency amplification and linearization techniques and numerous IEEE journal and conference papers. His research interests include silicon-based integrated circuits for radio frequency communications and deep learning AI-based radio systems for wireless AI communications. For more information: https://www.cud.ac.ae/personnel/dr-ziad-zouheir-el-khatib.

**FIRUZ KAMALOV** (Member, IEEE) received the B.A. degree in mathematics from Macalester College, USA, in 2004, and the Ph.D. degree in mathematics from the University of Nebraska–Lincoln (UNL), in 2011. In 2011, he joined Canadian University Dubai, where he has taught a wide range of mathematics courses across curricula. His research interests include C∗-algebras, functional analysis, machine learning, and data mining. While at UNL, he was a recipient of the Prestigious Othmer Fellowship, from 2005 to 2008, given to exceptional incoming scholars, and the DeWitt Wallace Distinguished Scholarship, from 2000 to 2004. He was also a recipient of the CUD Academic Research Award, in 2013, and the CUD Teaching Award, in 2013. He is a Managing Editor of *Gulf Journal of Mathematics*.

**SHERIF MOUSSA** (Member, IEEE) received the M.Sc. degree in electrical and computer engineering from the University of Waterloo, Canada, and the Ph.D. degree in electrical and computer engineering from the University of Quebec at Trois-Riviers, Canada. In 2007, he joined Canadian University Dubai (CUD), where he is currently an Assistant Professor with the School of Engineering. Prior to joining CUD, he was a Lecturer with the School of Engineering, Centennial College, Toronto, Canada. He is an active Researcher who published in many international journals and conferences related to his field. He serves as a reviewer and a technical committee member for many international conferences. He is the Winner of the 2015 CUD Research Excellence Award and the Founder of the Flagship CUD Robotics Club. For more information: https://www.cud.ac.ae/personnel/dr-sherif-moussa.

**ADEL BEN MNAOUER** (Member, IEEE) received the B.Sc. degree in computer science from École Supérieure des communications (SUP'COM) of Tunisia, in 1985, the M.Eng. degree in electrical and computer engineering from the University of Fukui, Japan, 1993, and the Ph.D. degree in electrical and computer engineering from Yokohama National University, Japan, in 1997. He was the Dean of the College of Computer Engineering and Information Technology, Dar Al Uloom University, from 2010 to 2011, then as the Vice-Dean of Research. He is currently a Professor of computer science with Prince Sultan University, Riyadh, Saudi Arabia. His research interests include applied AI and IoT, VANETs and FANETs, blockchain and cybersecurity, and edge/fog computing. His research portfolio is worth U.S. $3.7 million in research funding focused on harnessing the power of IoT-based ubiquitous healthcare, air quality, and structural health monitoring systems. He is active in chairmanship and journal editorial board, a TPC, and organization of scores of top-class international conferences and symposia. He is a Senior Member of the IEEE Communication Society. For more information: https://www.cud.ac.ae/personnel/dr-adel-ben-mnaouer.

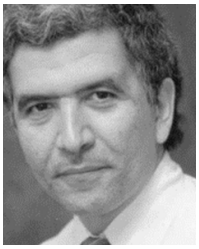

**MUSTAPHA C.E. YAGOUB** (Senior Member, IEEE) received the Dipl.-Ing. degree in electronics and the Magister degree in telecommunications from École Nationale Polytechnique, Algiers, Algeria, in 1979 and 1987, respectively, and the Ph.D. degree from the Institute National Polytechnique, Toulouse, France, in 1994. In 2001, he joined the School of Electrical Engineering and Computer Science (EECS), University of Ottawa, Ottawa, ON, Canada, where he is currently a Professor. His research interests include wireless communications systems design, RF/microwave CAD, RFID design, antenna design, active device modeling and characterization, neural networks for high-frequency applications, and applied electromagnetics. He is a Senior Member of the IEEE Microwave Theory and Techniques Society and a member of the Professional Engineers of Ontario, Canada, and the Ordre des ingénieurs du Québec, Canada.

**HALIM YANIKOMEROGLU** (Fellow, IEEE) is currently a Professor with the Department of Systems and Computer Engineering, Carleton University, Ottawa, Canada. His research group has made substantial contributions to 4G and 5G wireless technologies. His group's current focus is the wireless infrastructure for 2030s and 2040s. His extensive collaboration with industry resulted in 39 granted patents. He is a fellow of the Engineering Institute of Canada (EIC) and the Canadian Academy of Engineering (CAE), and a Distinguished Speaker for both the IEEE Communications Society and IEEE Vehicular Technology Society. He received the Best Paper Awards from the IEEE Competition on Non-Terrestrial Networks for B5G and 6G, in 2022, the IEEE International Conference in Communications (ICC), in 2021, and the IEEE Conference on Wireless for Space and Extreme Environments (WISEE), in 2021 and 2022. He received several awards for his research, teaching, and service.